LA-4174-TR

C.3

LOS ALAMOS SCIENTIFIC LABORATORY
of the
University of California
LOS ALAMOS • NEW MEXICO

Identification and Nuclear Spectroscopy of Several Short-Lived Fission Products with an On-Line Mass Separator

UNITED STATES
ATOMIC ENERGY COMMISSION
CONTRACT W-7405-ENG. 36

LEGAL NOTICE

This report was prepared as an account of Government sponsored work. Neither the United States, nor the Commission, nor any person acting on behalf of the Commission:

A. Makes any warranty or representation, expressed or implied, with respect to the accuracy, completeness, or usefulness of the information contained in this report, or that the use of any information, apparatus, method, or process disclosed in this report may not infringe privately owned rights; or

B. Assumes any liabilities with respect to the use of, or for damages resulting from the use of any information, apparatus, method, or process disclosed in this report.

As used in the above, "person acting on behalf of the Commission" includes any employee or contractor of the Commission, or employee of such contractor, to the extent that such employee or contractor of the Commission, or employee of such contractor prepares, disseminates, or provides access to, any information pursuant to his employment or contract with the Commission, or his employment with such contractor.

This translation has been prepared in response to a specific request; it is being given standard distribution because of its relevance to the nuclear energy program. Reasonable effort has been made to ensure accuracy but no guarantee is offered.

Printed in the United States of America. Available from
Clearinghouse for Federal Scientific and Technical Information
National Bureau of Standards, U. S. Department of Commerce
Springfield, Virginia 22151
Price: Printed Copy $3.00; Microfiche $0.65

Distributed: March 23, 1970

LA-4174-TR
UC-34, PHYSICS
TID-4500

LOS ALAMOS SCIENTIFIC LABORATORY
of the
University of California
LOS ALAMOS • NEW MEXICO

Identification and Nuclear Spectroscopy of Several Short-Lived Fission Products with an On-Line Mass Separator

by

J. Eidens

Dissertation submitted to the School of Mathematics and Natural Sciences, Technological College of Rhineland-Westphalia, Aachen, July 1968

Source: NP-17528, Nuclear Research Center, Jülich, Department of Solid State and Neutron Physics.

Translated by Kanner Associates

CONTENTS

IDENTIFICATION AND NUCLEAR SPECTROSCOPY OF SEVERAL SHORT-LIVED FISSION PRODUCTS WITH AN ON-LINE MASS SEPARATOR

by

J. Eidens

ABSTRACT

An apparatus for spectroscopy of short-lived fission products was constructed at the focal point of the helium-filled mass separator of the Jülich 2 research reactor. The separator mass calibration was obtained by γ radiation of known, long-lived fission products. The β-decay half-life of unknown short-lived fission products was determined on the basis of several high-intensity γ lines. Coincident β-γ spectra were recorded, and potentially occurring γ-γ cascades were obtained. The lines found could be assigned to eight nuclides for which the following β-decay half-lives and Q values were measured.

^{84}Se: (3.5 ± 0.1) min, (1.8 ± 0.1) MeV
^{91}Kr: (7.9 ± 0.5) sec, (5.7 ± 0.4) MeV
^{97}Y : (1.11 ± 0.03) sec, (5.7 ± 0.2) MeV
^{99}Nb: (14.3 ± 0.6) sec, (3.7 ± 0.2) MeV
^{99}Zr: (2.4 ± 0.1) sec, (4.5 ± 0.2) MeV
^{100}Nb: (6.6 ± 0.2) sec, (6.5 ± 0.3) MeV
^{101}Nb: (7.0 ± 0.2) sec, (4.6 ± 0.2) MeV
^{101}Zr: (3.3 ± 0.6) sec, (6.5 ± 0.7) MeV

In three instances, the half-life of the parent nuclides could be estimated from the decay curves as follows.

^{97}Sr: (0.4 ± 0.3) sec,
^{99}Y : (0.8 ± 0.7) sec,
^{100}Zr: (1.0 ± 0.9) sec.

1. INTRODUCTION

In nuclear physics there is great interest in those nuclides that are far from the bottom of the mass trough.[1,2] About 2,000 β-unstable nuclides with a half-life of greater than 10^{-2} sec should be expected. Only a few of these are known today. Nuclear spectroscopy of nuclei with high proton or neutron excess provides data which can be used to extrapolate theoretical expressions into the area of unstable nuclei in the slopes of the mass trough.

Nuclei with high proton excess can be produced with the aid of accelerators by bombarding stable nuclei with high-energy protons. There are no capture reactions which would lead to nuclei with a comparable high neutron excess. Only nuclear fission, e.g., thermal fission of ^{235}U, yields a large number of neutron-rich nuclei in the A = 80 to 160 mass range which, after volatilization of prompt neutrons, are still about three unit charges from the proton-neutron ratio of stable nuclei. These nuclides decay into stable nuclei through multiple β^- transitions.

Because of their high neutron excess, the fission products are high in the slope of the mass

trough; i.e., the Q values of the first β decay events are high, and the half-lives are correspondingly short. Half-lives of a few tenths of a second are the shortest that may be expected for fission products with significant yield. This is experimentally confirmed by Seyfarth[3] who recorded the mean β activity of the fission-product population as a function of time.

To perform nuclear spectroscopy of individual fission products, one must first separate the nuclide under study from the mixture produced in fission. For some chemical elements, such rapid chemical processes have been developed that separation times of only a few seconds are possible. For other elements, radiochemical methods are not applicable because such specific and rapid separation methods are lacking. For some time there have been projects that combine chemical and physical means for separating isotopes.[2] A selective chemical process, e.g., a gas-flux method, brings certain chemical elements from among the reaction products from the target to the ion source of an electromagnetic "on-line" separator. Some transport time and transport loss must always be accepted in a process of this type which works with moderated fission products.

On-line separators employing purely physical separation methods utilize the fact that fission produces fission products in the form of ions of such high ionic charge that they may be deflected in magnetic fields. However, the ionic charge for such nonmoderated fission products is not sharply delineated; rather, the ionic charge numbers of fission products of one mass form a distribution with a half-width of about 30%. In all mass spectrometers that separate according to the ratio of ionic charge number to mass, this leads to separation of individual masses into different ionic charge components. High resolving power of the apparatus is required for separation, and the resulting intensity yield is generally poor.

The gas-filled mass separator solves the difficulty of wide ionic charge distribution for nonmoderated fission products in a special manner. It permits "on-line" mass separation with high-intensity yield, although with only moderate mass resolution. It is well suited for nuclear measurement of fission products.

2. SEPARATION OF FISSION PRODUCTS BY GAS-FILLED MASS SEPARATOR

2.1. Separator Design

A gas-filled mass separator was first built by Cohen[4] at Oak Ridge, and later by Armbruster[5] at Munich. A new apparatus of this type, constructed during 1963 through 1966 for the Jülich 2 (Dido) research reactor, delivers a high thermal-neutron flux of $2 \cdot 10^{14}$ $cm^{-2}sec^{-1}$.[6] This apparatus is shown in Fig. 1. A 1-mg/cm^2 layer of ^{235}U at the hot end of an evacuated radiation-tube insert serves as the fission-product source with a source strength of $5 \cdot 10^{12}$ fission products per sec. The radiation-tube collimator defines a solid angle of magnitude $1.4 \cdot 10^{-6}$. The fission products falling into this solid angle are deflected from the neutron and γ-ray background outside the biological shield by a focusing magnet system, and are separated according to their mass. The strong neutron and γ beam is destroyed in a beam catcher. In the operating range of the magnetic field, the vacuum chamber is filled with several Torr of helium which is separated from the rest of the vacuum system by VYNS windows with a thickness of 70 μg/cm^2. Charge transfer collisions of fission products in helium permit velocity focusing and collection of all ionic charge states on one trajectory having a mean radius of curvature ρ. The fission-product flight time from the source to the separator focus is about 1 μsec. For the high-yield mass range, a corpuscular stream density of 10^4 fission products/cm^2/sec is obtained at the focal point.

The mass separator vacuum system is highly contaminated by krypton and xenon originating in the fission source. The pump exhaust gas enters the reactor exhaust canal only through a decontamination vessel that guarantees sufficient holdup time. When necessary, the gas may also be held back in pressure containers by means of a compressor. Vacuum pumps, storage containers, and compressors are located in a gastight compartment behind a lead shield in the bottom of the reactor. Helium pressure in the charge-transfer chamber is maintained by circulation. The gas inlet valve is regulated by a light barrier that scans the level of a U-type tube manometer filled with pump oil.

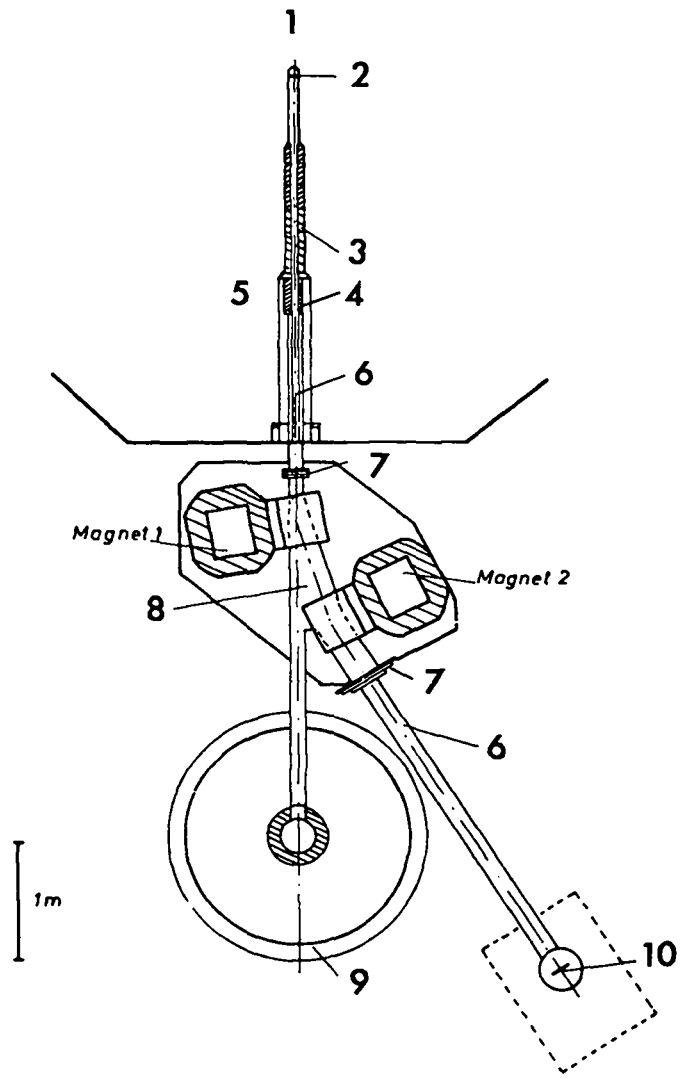

Key:

1 - Reactor core
2 - ^{235}U fission source
3 - Collimator
4 - Lock
5 - Biological shield
6 - Vacuum
7 - VYNS window
8 - Charge-transfer chamber, ~1-mm Hg helium pressure
9 - Beam catcher
10 - Image plane

Fig. 1. Gas-filled mass separator for fission products, at the Jülich FRJ-2 research reactor.

2.2. Operating Principle of the Separator

As fission products pass through the helium path, they transfer charges and their ionic charges assume an equilibrium distribution. According to a formula given by Heckman et al.[7] and empirically confirmed by Betz et al.,[8] the mean value, $\bar{q}$, of this distribution can be described by the expression

$$\bar{q} = Z\left[1 - C.\exp\left(-\frac{v}{v_o Z^{\gamma}}\right)\right] \quad , \qquad (1)$$

where Z and v denote nuclear charge and velocity of the fission product, and v_o is $\frac{11}{137}$ of the velocity of light. C and γ are experimentally fitted parameters.

In passing through a magnetic field with magnetic induction B, fission products of mass A are deflected into trajectories with a mean radius of curvature, ρ. Therefore,

$$B\rho \sim \frac{Av}{\bar{q}} \quad . \qquad (2)$$

For $c \approx 1$, which is fairly well satisfied, Eq. (1) may be approximated by

$$\bar{q} \approx \frac{v}{v_o} \cdot Z^{1-\gamma} \quad . \qquad (3)$$

Equations (2) and (3) yield the following approximate expression:

$$B\rho \sim \frac{A}{Z^{1-\gamma}} \quad . \qquad (4)$$

Fission products belonging to a mass chain A pass the deflection magnet with a mean primary nuclear charge Z_p; this is the centroid of primary nuclear charge distribution produced in fission. As long as this Z_p is an unambiguous function of A, the separator will actually sort out the fission products according to their masses.

$$B\rho = f(A) \sim \frac{A}{Z_p(A)^{1-\gamma}} \quad . \qquad (5)$$

In certain cases, advantage can be taken of the approximate proportionality of the fission products A and Z_p. One then obtains

$$B\rho \sim A^{\gamma} \quad . \qquad (6)$$

The dependence of the magnitudes of C and γ upon the atomic number Z is reflected by the fact that the simple power law of Eq. (6) can be approximated within small ranges only with a constant exponent. Consequently, we define an experimental quantity:

$$\Gamma = \frac{d(B\rho)/B\rho}{dA/A} \quad . \qquad (7)$$

This quantity gives the local gradient of the mass calibration curve $B = f(A)$, that is, the mass dispersion of the separator.

Of importance for the resolution of the mass separator is the variation of those ionic charge values that are obtained by averaging over the path length of each fission product in the charged gas stream, against the average value of the total equilibrium distribution, $\bar{q}$. Other contributions to the resolution are caused by the diffusivity of the beam by multiple scattering in the gas and in the VYNS windows, by the size of the source and the detectors, and by the distribution of nuclear charge, Z, about the average value of Z_p for fission products of one mass chain. In the light fission-product group, one can establish at optimum helium pressure a resolution of $\Delta(B\rho)/B\rho$ of about 4.3% as compared to 6.1% for the heavy fission-product group. These resolution values were determined by the method described below. The corresponding helium pressures in the charge-transfer chamber were 6.5 Torr for the light, and 1.3 Torr for the heavy fission products.

2.3. Gamma-Spectroscopy as a Tool for Identification of Individual Nuclides and Investigation of Separator Properties

The separator's moderate resolution can be illustrated by the degree of beam purity: in the light fission-product group, only 13% of all fission products collected at the focus belong to the equilibrium mass that corresponds to the chosen value of $B\rho$; the rest are neighboring masses that are not being sought.

Thus, the beam arriving at the collector always consists of a mixture of fission products with a certain mass range. To identify fission products of a specific mass, i.e., to identify individual nuclides of a specific mass chain in this mixture, we make use of their radioactive properties. With the Munich separator, Hovestadt[9-11] used a nuclear spectroscopy process that allowed him to analyze the half-life and energy of a single γ line in the multitude of radioactive sources. Because of the moderate separator resolution, the γ line of a specific nuclide is not found only at the $B\rho$-value corresponding to its mass; rather, the γ-line intensity distribution plotted against $B\rho$ produces a Gaussian curve with a half-width of 4.3%. By systematic search for strong γ lines at different $B\rho$ values, one can obtain a separator mass calibration on the basis of identifiable, known γ lines, whereas the unknown lines must be attributed to new nuclides.

Conversely, spectroscopy may be used to investigate ion physics properties of the mass separator. The experimental line configuration and its half-width, i.e., the $B\rho$ resolution, were measured in the charge-transfer chamber as a function of helium pressure.[6] The resolving power of the apparatus for other gases was similarly investigated. This method may also be used to determine the parameters C and γ in Eq. (1) which are

a function of the nuclear charge number of the fission products and of the transfer medium. Grueter[12] performed part of these ion physics investigations in preparing a Master's Thesis.

2.4. Apparent Mass Shift of Primary Fission Products

In Eq. (5) which expresses Bρ solely as a function of mass A, we assumed that the same average $Z_p(A)$ applies to all fission products of a mass chain passing through the deflecting magnets. However, this is correct only for secondary fission products, i.e., for those nuclides produced not in fission, but by β decay of primary parent nuclides only at the separator collector. The term "primary fission products" refers to the fission products present after volatilization of prompt neutrons. When fission-product activity is measured in hours or minutes, we are dealing exclusively with secondary fission products.

If, however, the investigation is extended into the half-life range of seconds, then we deal more and more with primary nuclides. We are then in part investigating nuclei that have already passed through the deflecting system with their own Z, rather than nuclei that all pass through the deflecting system with the Z of their even shorter-lived parent nuclei. The average $\bar{Z}$ corresponding to this mixture, which according to Eq. (4) applies to deflection, will then always be smaller than Z_p, i.e., smaller than the average for all primary nuclear charges of the mass under study.

As a result, the centroid of the intensity distribution of such primary nuclides will appear at higher values of Bρ; i.e., the mass indicated is too high.

Correct allocation of primary fission products requires a quantitative estimate of this apparent mass shift. Equation (2) yields the total differential in logarithmic form:

$$d\ln(B\rho) = d\ln A + d\ln v - d\ln \bar{q} \quad . \tag{8}$$

With the general argument $\bar{q} = \bar{q}(v,z)$, we obtain:

$$d\ln(B\rho) = d\ln A + d\ln v - \frac{\delta \ln \bar{q}}{\delta \ln Z} d\ln Z - \frac{\delta \ln \bar{q}}{\delta \ln v} d\ln v \quad . \tag{9}$$

But A and Z are approximately proportional for fission products; i.e., $d\ln A \approx d\ln Z$. For the velocity spectrum of fission products in the separator, $\bar{q}$ is, furthermore, approximately proportional to v, so that $\frac{\delta \ln \bar{q}}{\delta \ln v} = 1$. This leads to the expression:

$$d\ln(B\rho) = \left(1 - \frac{\delta \ln \bar{q}}{\delta \ln Z}\right) d\ln A \quad . \tag{10}$$

According to Eq. (7), the slope of the mass calibration curve is described by

$$\Gamma = \frac{d\ln(B\rho)}{d\ln A} \quad . \tag{11}$$

Equations (10) and (11) yield

$$\Gamma - 1 = -\frac{\delta \ln \bar{q}}{\delta \ln Z} \quad . \tag{12}$$

Considering a Bρ variation in the total differential of the form of Eq. (9) which is caused by variation of Z only (with A held constant), we find, again with the approximation $\frac{\delta \ln \bar{q}}{\delta \ln v} = 1$,

$$d\ln(B\rho)_{A=\text{const}} = -\frac{\delta \ln \bar{q}}{\delta \ln Z} d\ln Z \quad . \tag{13}$$

According to Eq. (11), this variation in Bρ corresponds to an apparent mass variation in the mass calibration curve:

$$d\ln A = \frac{d\ln(B\rho)}{\Gamma} \quad , \tag{14}$$

or, by use of Eqs. (12) and (13),

$$d\ln A = \frac{\Gamma - 1}{\Gamma} d\ln Z \quad , \tag{15}$$

$$dA = \frac{\Gamma - 1}{\Gamma} \frac{A}{Z} dZ \quad . \tag{16}$$

The difference $\Delta Z = \bar{Z} - Z_p$ discussed above is substituted for dZ. To evaluate this expression, the shape of primary charge distribution and the position of its average Z_p must be known as a function of fission-product mass. According to Wahl,[13] the distribution was assumed to be a Gaussian function according to $\exp\left[-(Z-Z_p)^2/0.86\right]$.

The values of Z_p are computed from the equation

$$Z_p = Z_{UCD} \pm \Delta \quad , \tag{17}$$

where the positive sign applies to light, and the negative sign to heavy, fission products. Z_{UCD} (unchanged charge density) is given by

$$Z_{UCD} = \frac{92}{236}\left[A + \nu(A)\right] \quad , \qquad (18)$$

where $\nu(A)$ denotes the number of volatilized prompt neutrons. Milton and Fraser's results,[14] when corrected for the proper total number of prompt neutrons given by Reisdorf,[15] are considered the best experimental values available for the number of volatilized prompt neutrons. From Reisdorf and Armbruster's measurements,[15,16] the Δ value is set at 0.55 independent of mass to best approximate the earlier experimental result. More recent, unpublished measurements with the Jülich mass separator yield a Δ of 0.40 which is only slightly dependent on mass; however, we have not used this numerical value in performing the calculation.

From the data given and from the slope value Γ, one can compute the apparent mass shift in the mass separator for any primary fission product.

3. A CYCLICALLY OPERATING TRANSPORT BAND FOR FISSION-PRODUCT DECAY MEASUREMENT

3.1. Separation of Irradiation and Measurement Locations

In principle, one could position a detector device for nuclear spectroscopy directly at the target in the separator focus. However, such an arrangement would have the following disadvantages. For decay measurements, the target would have to be irradiated for some time, then the fission-product beam would have to be turned off by means of a shutter to allow investigation of the decaying activity at the target. Use of this method in cycles gave only 50% time utilization of the fission-product beam supplied by the mass separator. Furthermore, particularly strong background from scattered γ quanta that hit the target from the same direction as the fission products, and which therefore cannot be screened out, will have to be expected at the focus, which is at the same elevation as the collimator opening of the radiation tube insert. Finally, the vacuum tube through which the fission products approach constitutes a heavy space limitation on design of a detector system which should approximate 4π geometry as nearly as possible.

For these reasons it is advisable to separate the irradiation and measurement locations. Here, the detector is $\sim$ 25 cm above the focus. The applied activity is transported to that point by an intermittently moving, cyclically operating transport band.

3.2. An Intermittently Operating Transport Band

Hovestadt[9] separated irradiation and measurement sites by means of an intermittently operated transport band. The method of operation is as follows: the transport band is at rest for a preselected period of irradiation or "cycle duration." During this time, a 32-mm^2 section of the band is irradiated with fission products. This section is then suddenly brought to the measurement location. While the fission-product decay events are being registered there, generally with the measuring period divided into several intervals, a new section of the transport band is being irradiated at the focus. This process is repeated at a constant Bρ value until statistical data for the recorded decay spectra are sufficient.

Fig. 2 shows the transport-band layout. For the sudden, rapid band transport, Hovestadt[9] used a system of electromagnetically operated slip clutches, brakes, and blocking pins which were difficult to operate in a vacuum chamber. At Jülich, the axles of all vehicles required for band movement were, therefore, carried to the outside through vacuum rotary transmissions. The rapid-transport wheel is driven by a cross wheel. The cross wheel is driven by an eccentric crank gear, so that only 10% of one gear rotation is needed for a quarter turn, instead of the usual 25%. During the other 90% of the gear rotation, a delivery loop is wound off the lower drum to provide the necessary band length for subsequent rapid transport. The loop formed above by the preceding rapid transport is simultaneously wound onto the upper drum. During the fastest measuring-chamber operation, 0.1 sec is required for rapid transport from the irradiation to the measurement location; this may be repeated once per second.

The choice of optimum cycle duration is governed by the half-life of the nuclide under study. Although nuclides whose half-lives are small compared to irradiation time are being accumulated at the irradiation site until saturation, they decay

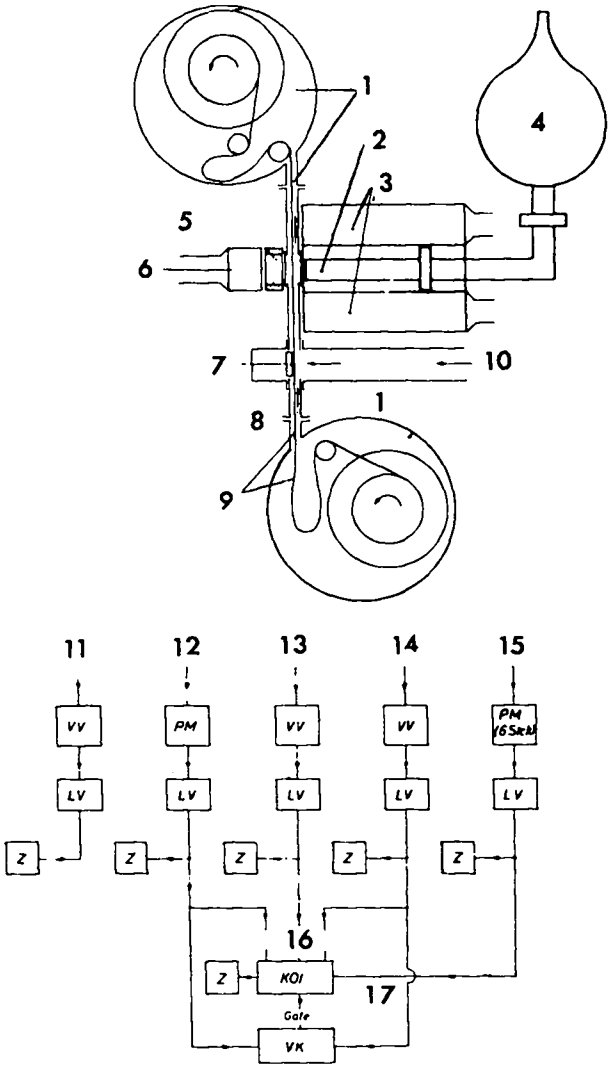

Key:

1 - Vacuum chamber
2 - Ge(Li)-diode
3 - NaI(Ti) anti-Compton ring crystal
4 - Dewar vessel
5 - β-transmission counter, anthracene β crystal
6 - Measurement location
7 - Irradiation location
8 - Fission-product monitor (semiconductor detector)
9 - Intermittently operated transport band
10 - Fission-product beam
11 - From fission-product monitor
12 - From β crystal
13 - From β counter
14 - From Ge diode
15 - From ring crystal
16 - Coincidence
17 - Anticoincidence
VV - Preamplifier
PM - Photomultiplier with emitter follower
LV - Linear amplifier
Z - Counter
KOI - Quadruple coincidence stage
VK - Two-parameter multichannel analyzer

Fig. 2. Test setup for nuclear spectroscopy of short-lived fission products.

rapidly at the beginning of the measurement period, and do not contribute further to total activity. Conversely, for nuclides whose half-lives are long compared to irradiation time, saturated activity is not even reached at the irradiation site. The yield, h, is defined as the ratio of the number of nuclei of a nuclide which decay during the measurement period in front of the detector device, to the number of nuclei of the same nuclide which are being applied to the transport band during the irradiation period. Hovestadt has computed yield functions for various cycle durations and measurement intervals relative to half-lives. When the measurement period extends over the full cycle, one can obtain an optimum yield of 40% by choosing an ~1:2 ratio of half-life to irradiation period. Figure 3 gives the yield function for an example in which the measurement interval begins after 14% of cycle duration, and ends at 90%. The yield is about 30% with optimum adjustment of the ratio of half-life to irradiation period.

The time discrimination properties of the intermittently operated transport band described by the yield function permit rough separation of fission-product activities with respect to their half-lives.

3.3. The Detector System

Figure 2 shows the detector system at the measurement location. The principle of Hovestadt's

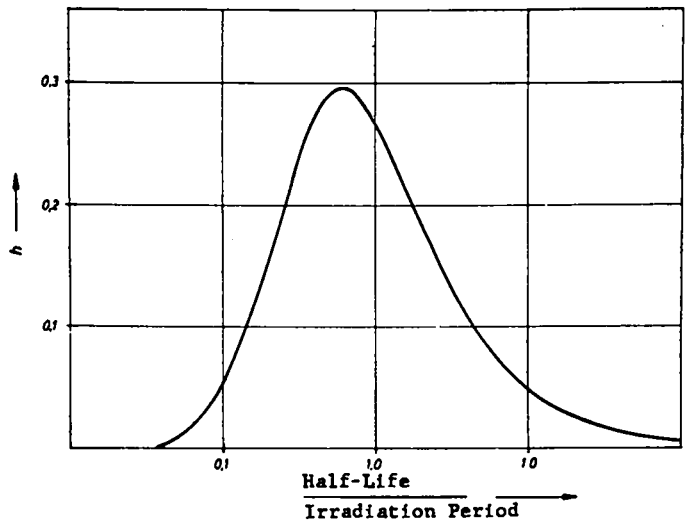

Fig. 3. Yield function, h, of the intermittently operated transport band for a measuring time of 14 to 90% of cycle duration.

method[9,10] used here for identification of fission products, consists of registration, by β-γ coincidence measurement, of the characteristic γ radiation emitted by an excited state after it is populated by β decay. This coincidence method has the advantage of suppressing the strong γ background of the reactor hall. The β signal is provided by a β counter, whereas a Ge(Li)-diode serves as γ detector. Between these, the transport band is located in a small vacuum chamber that has two Hostaphan windows with a surface density of 11 mg/cm^2 at the measurement location.

The Ge detector has a detection-sensitive volume of almost 20 cm^3 and, with the electronic equipment used (see Sec. 3.4), gave an energy resolution of 5.5 keV for the 1330-keV ^{60}Co line. The detection probability integrated over the photopeak was absolutely determined for the existing geometry; for 1330-keV γ energy it is $1.0 \cdot 10^{-3}$.

The Ge diode is connected to the corresponding Dewar vessel through a specially built, long cold finger, so that the diode can be used inside an anti-Compton ring crystal. This 12-in.-long by 9-in.-diam NaI scintillation crystal has a 3-in.-diam central through bore. Six photomultipliers are mounted in a circle on one face. The crystal is connected in anticoincidence to the Ge diode. Thus it reduces the Compton background in the spectrum, because all events in which a γ quantum Compton-scattered in the Ge diode is detected in the surrounding ring crystal are negated by the anticoincidence condition. Suppression of the Compton peak is especially important as the γ spectra are very complex because of the main nuclei simultaneously irradiated onto the transport band. However, the geometry used is not designed for optimum Compton repression, but rather for maximum Ge diode detection probability. Depending on the spectrum, the repression factor ranges from 2 to 4.

For γ quanta not derived from a Compton process in the Ge diode but coming directly from the irradiated transport band, the ring crystal has a total detection probability (i.e., a detection probability integrated over the photopeak and the Compton peak) of $2 \cdot 10^{-1}$; from 0 to 1300 keV, the detection probability is practically independent of energy. Accordingly, two γ lines of a γ-γ cascade attenuate each other in the Ge diode spectrum by the ratio of their emission probabilities multiplied by $2 \cdot 10^{-1}$ because of the anticoincidence condition. Finally, the entire ring crystal must be surrounded with heavy lead sheathing to shield it from the high γ background in the reactor hall, because all γ quanta hitting the large-volume ring crystal produce anticoincidence signals which, in case of a high rate, would lead to high dead-time losses of the coincidence array.

An anthracene crystal β scintillator is located on the other side of the transport band be-

hind the transmission-counter-type β counter. The anthracene crystal allows recording of β spectra coincident to the γ lines. Here the coincidence system of the β transmission counter and the β crystal forms a β spectrometer of low γ sensitivity as described by Armbruster and Specht.[17] For the 976-keV ^{207}Bi conversion electrons, the anthracene crystal attains a β-energy resolution of 150 keV. The crystal is 1-in. thick, sufficient to safely absorb 7.5-MeV β particles. The crystal diameter is 2.5 in. To reduce fringe effects that might distort the spectrum, a 40-mm-diam steel diaphragm is mounted between the transmission counter and the crystal.

A silicone boundary layer counter is located inside the vacuum in the irradiation section of the test chamber. This semiconductor detector registers the fission products that pass through the transport band perforations, and thus monitors the permanency of the fission-product beam supplied by the separator.

3.4. Electronic Equipment and Control

Figure 2 includes a block diagram of the electronic equipment used. The pulses of the Ge diode, β counter, and fission-product monitor are transmitted through charge-sensitive preamplifiers to their respective linear amplifiers, and the NaI ring crystal and anthracene crystal signals are transmitted to their respective linear amplifiers through photomultipliers with emitter follower stages. The single counting rates of all five branches are recorded in counters for control purposes. The amplifier outputs from the β crystal, β counter, and Ge diode are given in coincidence to a multicoincidence box, and that from the ring crystal is given in anticoincidence. The multicoincidence box is operated with a 0.2-μsec coincidence resolution period. The multichannel analyzer gate is opened by the coincidence signals which are recorded in a control counter. The analog signals from the Ge diode and anthracene crystal can be stored in the 4096-channel analyzer in one- or two-dimensional operation. The electronic pulse equipment is of conventional design except that the Ge diode requires a special low-background branch consisting of a FET-preamplifier, Tennelec Model TC 130, and a main amplifier, Tennelec Model TC 200.

Overall control of the cyclically repeated irradiation and measurement processes is by an external electronic clock set to the desired cycle duration. With a time scanner having units of 1% of cycle duration, pulses may be taken off to address a system of univibrators or flip-flop multivibrators. The testing process can then be programmed by means of socket-switch connections: the transport process is initiated, the multichannel analyzer and the counters are turned on, or the multichannel analyzer is reset for storage in another memory section. The number of cycles during which the irradiation and measurement process is to be repeated for a constant value of Bρ can be set by mechanical preselection counters. Thereafter, the deflecting magnet power supply is switched to the next step, and the multichannel analyzer memory is printed out, always one cycle later.

4. RECORDING AND ANALYSIS OF FISSION-PRODUCT β-COINCIDENT γ SPECTRA

4.1. Measurement Method and Data Evaluation

A nuclide can be identified if it emits a strong β-coincident γ line whose intensity can be recorded as a function of the Bρ value. However, a multitude of nuclides are always simultaneously present at the detector. This is due partially to the moderate separator resolution, and partially to the low time discrimination of the transport band. Use of a Li-drifted Ge diode as γ detector, instead of a NaI crystal such as Hovestadt[9,10] used in Munich, therefore proved not only advantageous, but also unavoidable because the γ detector must be able to distinguish between the two γ evergies when two nuclides with γ lines of similar energy exist at neighboring masses. Only in that case can the intensity distribution plotted against Bρ be separated into two Gaussian lines, which is the prerequisite for differentiation and classification of the nuclides. With a NaI crystal, this is possible only in a few favorable cases because the crystal's energy resolution is one order of magnitude inferior to that of the Ge diode used here.

We first attempted a test series of the same extent as that subsequently described for the Ge detector with a NaI crystal that was being used in conjunction with the anti-Compton ring crystal.

However, we could not obtain results that would lead substantially further than those obtained by Hovestadt at Munich, despite suppression of Compton peaks in the spectra and the fact that the fission-product beam at Jülich was 10 to 20 times more intense that that at Munich.

Conversion of the apparatus to the 20-cm^3 Ge diode resulted in a factor of 50 loss in detection probability integrated over the photopeak compared to the 3-in.-diam by 5-in.-long NaI crystal previously used. This intensity loss is fully effective, for instance, in recording a β spectrum coincident to a γ line, because the coincidence rate is determined by the integral over the photopeak. It is less detrimental in evaluation of one-dimensional γ spectra, where it is primarily important that the line be clearly distinguishable from the background in the spectrum. The Ge diode half-width is smaller, e.g., at 1330 keV it is reduced by a factor of 13 compared to that of the NaI crystal; accordingly, the peak height decreases by only a factor of four.

To find the strong β-coincident γ lines for 12 Bρ values corresponding to the light fission-product mass range, and 11 values corresponding to the heavy fission-product mass range, we recorded and registered the Ge-detector spectra one-dimensionally in the multichannel analyzer. For this purpose, the Ge diode and β counter were connected in coincidence, and the ring crystal in anticoincidence. We used the transport-band time discrimination by covering the Bρ range in four separate test series with cycle durations of 130 min, 8 min, 30 sec, and 2.1 sec. Here the two test series with longer cycles furnish essentially the γ lines emitted by longer-lived fission products in the range of hours and minutes, so that a separator mass calibration, i.e., the curve $B\rho = f(A)$, can be obtained. The two short-duration test series enter into the range of seconds-long half-lives which contains many as yet unknown nuclides.

The number of cycles, for which we repeated irradiation and measurement at constant Bρ values, was as follows: for the 130-min run, 3 to 10 cycles; for the 8-min run, 30 to 170 cycles; for the 30-sec run, 600 to 2500 cycles; and for the 2.1-sec run, 6000 to 18,000 cycles. Accordingly, the measurement periods for a particular Bρ value always ranged from ~4 to ~20 h. They were roughly fitted to the beam intensity at the focus, which varies for the different mass ranges depending on fission yield.

The γ spectra supplied by the Ge detector were stored in the multichannel analyzer so that about a quarter of the analyzer memory, or 1024 channels, was available for the 0- to 2-MeV γ-energy range. The test period within each cycle was subdivided into four equal intervals. The pulses were accordingly stored one after the other in different memory sections. Accordingly, we obtained four partial spectra for each Bρ value in each test run; these describe the time decay of activity and permit rough half-life analysis of the γ lines present. After completion of the preselected number of cycles, the four spectra stored in the 4096 analyzer channels were automatically printed out on punched tape. The punched tapes were read into an IBM 1401 computer with a plot program. The computer plotted the spectra directly onto 60-cm^2 sheets. About 300 spectra were processed. Figure 4 is a typical plot.

With the division of the multichannel analyzer described above, the γ-energy difference per channel is about 2 keV. With the 5.5-keV energy resolution this leads to needle-shaped photopeaks. A computer program for automatic search and evaluation of such peaks was not yet available. Therefore, we evaluated the plotted spectra by hand through graphical integration of the photopeaks. In so doing, we could determine the channel number of the line centroid to ± 1 channel, corresponding to ± 2 keV. The γ-detector energy calibration performed with conventional γ-calibration specimens also showed time variations of ± 1 channel, corresponding to ± 2 keV. Accordingly, a ± 3-keV error in energy determination is assumed for all γ lines.

The line intensities obtained by integration over the photopeak after the background is subtracted were plotted against Bρ using γ energy as the parameter, separately for each test run and for each quarter of a measuring interval. For clean, nonintermingling lines, the intensity distribution represents Gaussian distributions of about 4.3% and 6.1% half-width for the light and heavy fission-product groups, respectively.

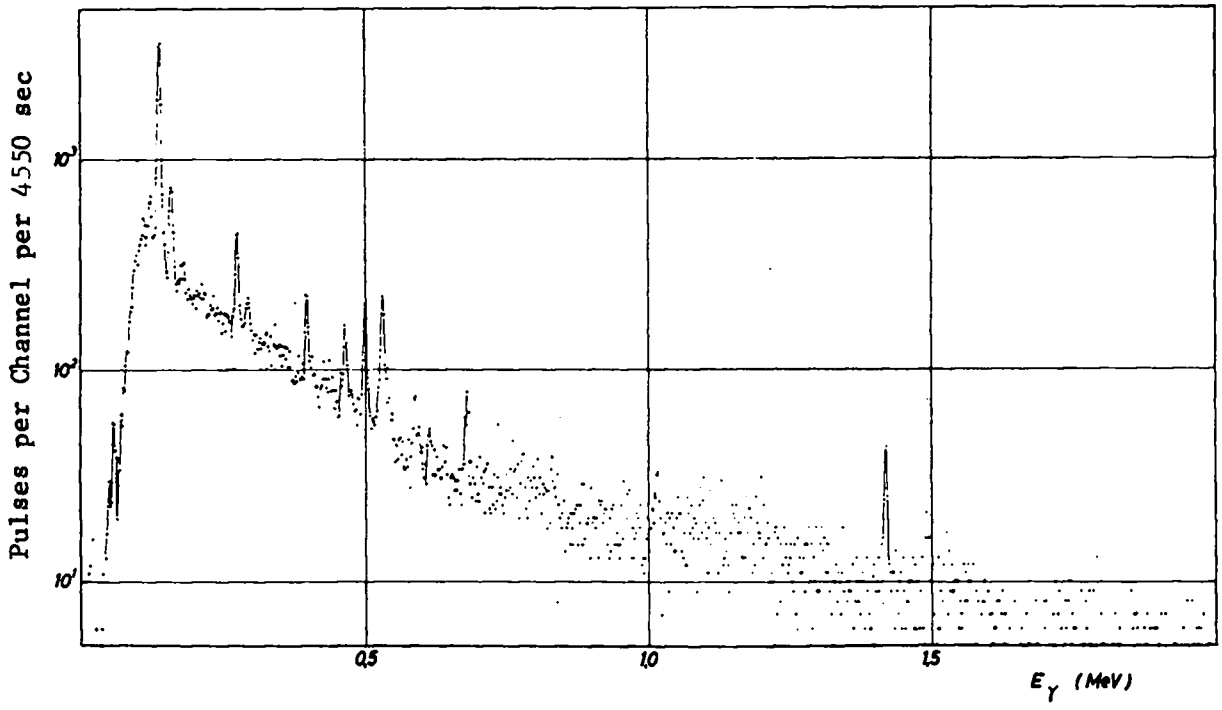

Fig 4. Example of β-coincident γ spectrum.

The peak of this Gaussian distribution represents the Bρ value of the respective γ line. The smallest line intensity clearly distinguishable in a single spectrum, and whose maximum in the Bρ distribution can still be determined, is ~1/min. Figure 5 is an example of the intensity distribution of a strong γ line plotted against Bρ, separately for the four quarters of the measuring interval.

Let us summarize the conditions for occurrence of strong, β-coincident γ lines. The emitting nuclides must have significant fission yield, β decay must not primarily lead immediately to the ground state of the daughter nucleus, and the β-γ transitions should not branch too much into different energy levels and different cascades.

4.2. Identified, Known γ Lines of Long-Lived Fission Products

Using the method described above, we found a number of γ lines which could be attributed to known nuclides on the basis of their energy and of rough half-life analyses. Their Bρ value could thus be used for mass calibration, i.e., to plot the curve Bρ = f(A). These nuclides are summarized in Tables I and II. The tables give first the test run in which the line was found, then the γ energy

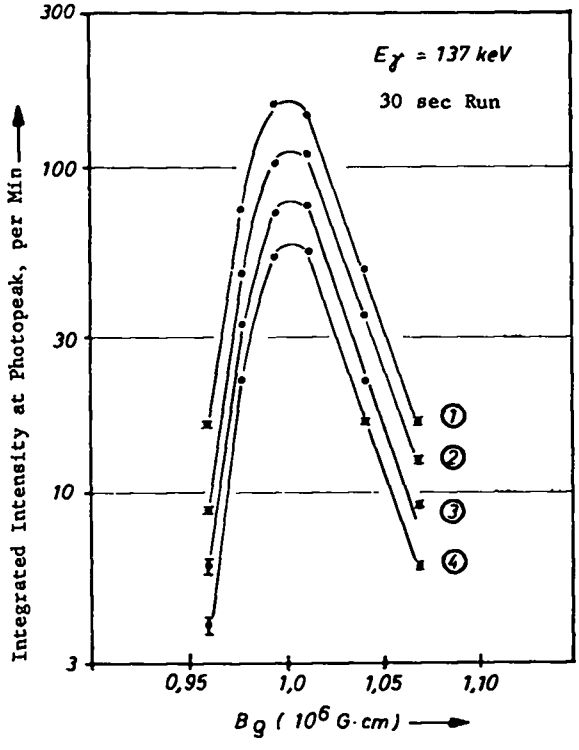

Fig. 5. Example of Bρ distribution of a strong γ line for the following measuring intervals:

(1) 3.3 to 9.9 sec after end of irradiation
(2) 9.9 to 16.5 " " " " "
(3) 16.5 to 23.1 " " " " "
(4) 23.1 to 29.7 " " " " "

TABLE I

IDENTIFIED KNOWN NUCLIDES IN THE LIGHT FISSION-PRODUCT GROUP

Nuclide	Test Run	γ-Energy Found (keV)	Reference
^{83}Se	130 min	354	18
^{84}Br	130 min	878	18
^{85m}Kr	130 min	150	18
^{87}Kr	130 min	403	18
^{88}Kr	130 min	166, 195, 1840	18
^{88}Br	30 sec	795	19
^{89}Rb	130 min, 8 min	1030, 1245	20
^{89}Kr	8 min	218, 494, 575	21
^{90}Rb	8 min	830	18
^{90}Kr	8 min, 30 sec	122, 240, 1118	22
^{91}Sr	130 min	749, 1022	18
^{91}Rb	8 min	95	23
^{92}Sr	130 min	1380	18
^{93}Y	130 min	268	18
^{93}Sr	8 min	258, 707, 886	24
^{94}Y	130 min, 8 min	916	18
^{94}Sr	8 min, 30 sec	1426	11
^{97}Nb	130 min	653	18
^{101}Tc	130 min, 8 min	302	18
^{101}Mo	130 min	588	18
^{103}Tc	8 min	136, 210, 343	25
^{104}Tc	130 min, 8 min	356	25
^{105}Ru	130 min	722	18

TABLE II

IDENTIFIED KNOWN NUCLIDES IN THE HEAVY FISSION-PRODUCT GROUP

Nuclide	Test Run	γ-Energy Found (keV)	Reference
^{131}Te	130 min, 8 min	149	18
^{133}Te	130 min	412	26
^{134}I	130 min	849, 886	18
^{135}Xe	130 min	256	18
^{138}Cs	130 min	467, 1015, 1440	18
^{139}Ba	130 min	170	18
^{141}Ba	130 min	193	27
^{145}Ce	8 min	726	18

measured, and, finally, the reference used in making the nuclide correlation.

4.3. Preparation of Mass-Calibration Curve and Description of Mass Dispersion and Resolution

The characteristic separator properties measured are shown in Figs. 6 and 7 for the light and heavy fission-product groups, respectively. The data apply to optimum helium pressures of 6.5 and 1.3 Torr in the charge-transfer chamber for the light and heavy fission products, respectively.

The bottom section of Fig. 6 shows the mass calibration curve $B\rho = f(A)$ obtained when the measured $B\rho$ values of the nuclides listed in Table I are plotted. This curve permits mass correlation of new nuclides by use of the $B\rho$ value of their γ lines. The mass calibration curve becomes steadily flatter with increasing mass. It cannot be described by a constant exponent γ in the exponential relationship of Eq. (6) in Sec. 2.2. The curve shape is determined by the relationship of the variables γ and C to the nuclear charge Z (see Eq. (1), Sec. 2.2). The second curve from the bottom in Fig. 6 shows the mass dispersion, Γ, as defined in Eq. (7). The points and errors shown were obtained by making a straight-line fit through every five points of the mass calibration curve to determine the local slope of Γ. The curvature of the mass calibration curve is a reflection of the fact that the mass dispersion decreases markedly in passing from lighter to heavier masses.

The third curve in Fig. 6 shows the measured $B\rho$ resolution of the separator. The measured half-width of the γ-line intensity has been plotted against $B\rho$. The intensity distribution against $B\rho$ could not be followed far enough to read a half-width for all γ lines that could be used for mass

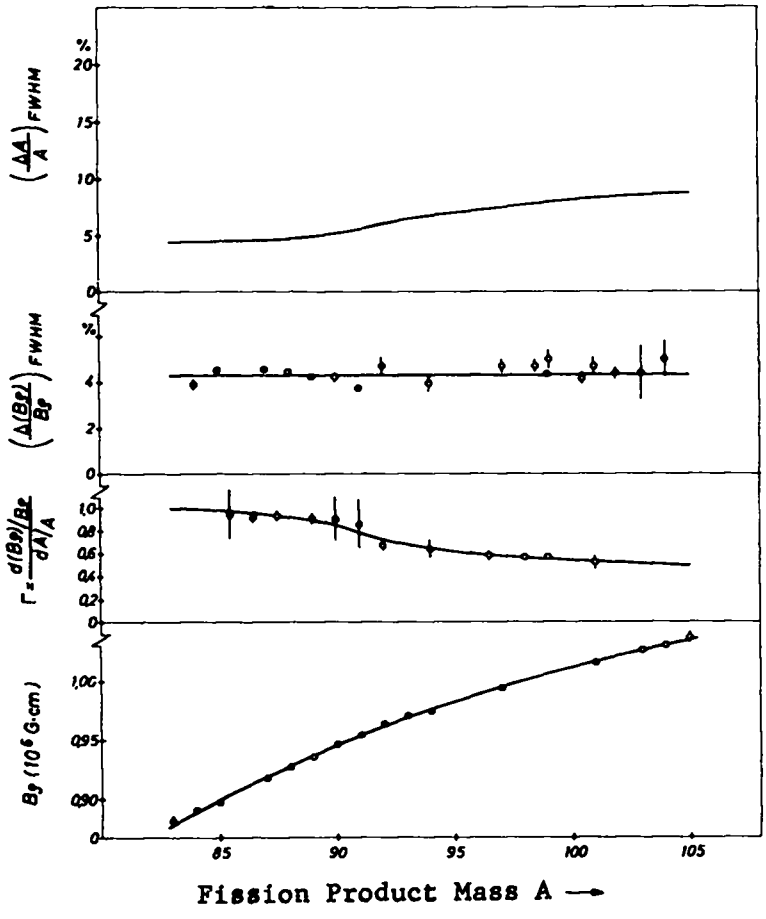

Fig. 6. Mass calibration curve, mass dispersion, $B\rho$ resolution, and mass resolution (bottom to top) for light fission products at 6.5-Torr helium pressure.

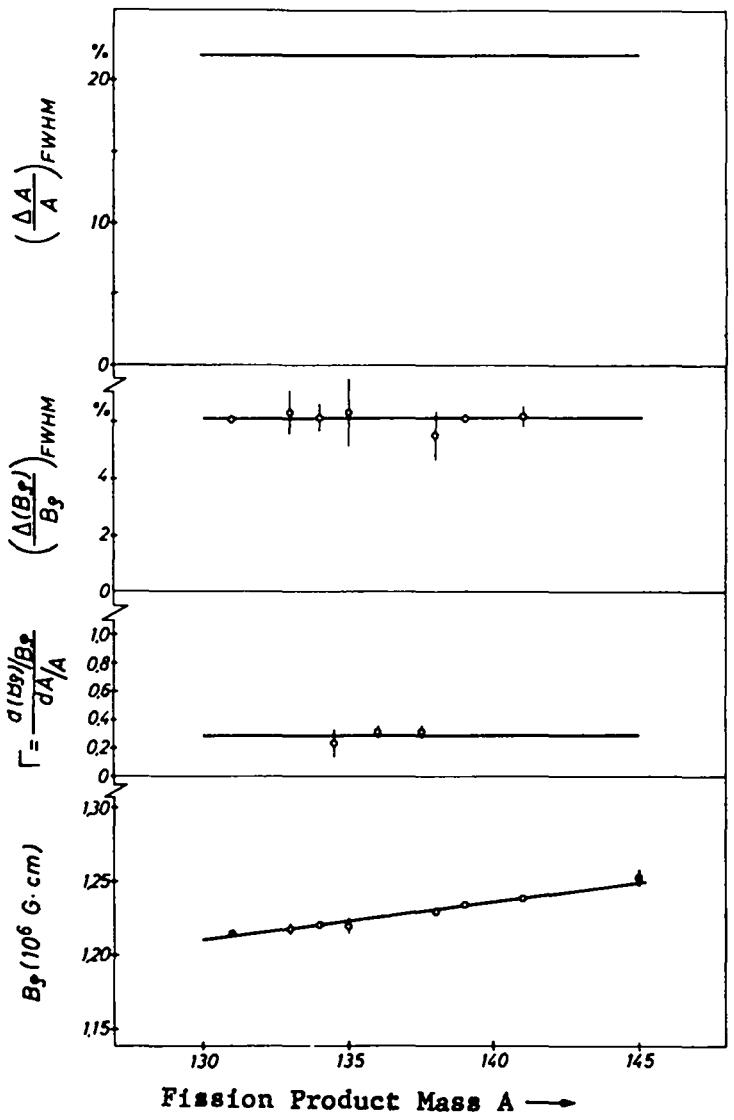

Fig. 7. Mass calibration curve, mass dispersion, Bρ resolution, and mass resolution (bottom to top) for heavy fission products at 1.3-Torr helium.

calibration. On the other hand, half-widths are also shown for new γ lines which will be discussed later. These appear in part at A values which are not integers because of the apparent mass shift discussed in Sec. 2.4. For the light fission-product group, the Bρ resolution is found to be 4.3%, independent of mass.

The upper curve of Fig. 6 shows the mass resolution of the separator, ΔA/A, obtained by dividing the Bρ resolution into Δ. Mass resolution capacity in the mass range of light fission-products is degraded from 4.4% for lighter, to 8.8% for heavier, masses. The mass resolving power values easily show that there is always a considerable mixture of neighboring masses with the desired mass.

Figure 7, similar to Fig. 6, shows the four corresponding curves for the heavy fission-product group. While 6.1% Bρ resolution is not significantly inferior to that in the light fission-product group, the average mass dispersion, Γ, is 0.28 so that only ~22% mass resolution results. The poor mass dispersion and mass resolution are the reason why only relatively few nuclides of the heavy fission-product group could be identified. The mass calibration curve could therefore be prepared only for a narrow mass range.

4.4. Strong, Unknown γ Lines of Short-Lived Fission Products in the Light Group

Since the mass-separator properties for the heavy fission-product group were appreciably less favorable than those for the light group, it seemed futile to extend the search for new, unknown γ lines of heavy fission products. We therefore ran the 30-sec and 2.1-sec tests only for Bρ values corresponding to light fission-product masses.

We found many unknown lines of different intensity in these two test runs. For further investigation, we had to perform triple coincidence experiments on these lines, as described in Sec. 5. For intensity reasons, we selected 12 nonintermingling lines which, at their maximum Bρ distribution, were found at a rate of at least 5/min. The strongest γ line investigated had a frequency of 160/min. Table III lists (a) the line energy (b) the test run in which it was observed, (c) the half-life estimate from rough half-life analysis, and (d) the apparent mass, A_{sep}, simulated by the separator, which follows from the Bρ value of the γ line.

5. FURTHER INVESTIGATION OF UNKNOWN γ LINES

5.1. Half-Life Measurement

To further investigate unknown lines in the light fission-product group, we adjusted the mass separator to the best operating condition for each line. The magnetic field was adjusted and held constant, so that the Bρ value corresponded to the maximum intensity distribution of the line. The transport band was operated at the best cycle duration, i.e., at about twice the half-life already roughly determined.

The simplest measurement performed for the new lines was an exact half-life analysis. The method described in Sec. 4.1 gave only a rough indication of half-life behavior, because the measuring interval during which the transport band remains in front of the detectors was divided into only four quarters. For exact measurement, we divided the 4096-channel analyzer into 16 subgroups of 256 channels each. By use of the electronic clock, the subsequent 16th of the multichannel analyzer was always addressed after 1/16th of the measuring interval during each cycle. The electronic equipment was set so that the part of the β-coincident γ spectrum containing the line under study would fall into the 256 available analyzer channels.

Depending on intensity, the measuring interval per line was between 2 and 15 h. Up to 27,000 cycles were counted for short-lived, low-intensity lines. After completion of each measurement, the data were printed out by the multichannel analyzer printer, and the integral of the photopeak line intensity was evaluated by hand after deduction of background for each of the 16 subgroups.

The test results are shown in Sec. 7 with the discussions of individual nuclides. The acti-

TABLE III

NEW γ LINES INVESTIGATED IN THE LIGHT FISSION-PRODUCT GROUP

γ-Energy (keV)	Test Run	$T_{1/2}$	A_{sep}
111	30 sec, 2.1 sec	ca. 8 sec	90.9 ± 0.3
125	2.1 sec	ca. 1 sec	97.6 ± 0.3
137	30 sec	ca. 13 sec	98.8 ± 0.2
159	30 sec	ca. 6 sec	100.9 ± 0.7
273	30 sec	ca. 6 sec	101.7 ± 0.7
293	30 sec	ca. 4 sec	102.0 ± 0.6
399	30 sec	ca. 5 sec	100.4 ± 0.6
406	8 min	ca. 3 min	84.2 ± 0.2
468	30 sec, 2.1 sec	ca. 2 sec	98.6 ± 0.7
548	2.1 sec	ca. 3 sec	98.3 ± 1.0
595	2.1 sec	ca. 3 sec	99.0 ± 0.7
810	2.1 sec	ca. 1 sec	96.6 ± 0.7

vity decay is shown as a function of time; here we chose the end of irradiation of the transport band, i.e., the beginning of rapid transport, as zero time. We computed half-lives from the decay curves by use of a computer program (weighted least-squares fit). For some γ lines, the semi-logarithmic plot of the decay curves shows a clear curvature at the start, caused by the nuclide being built up from its parent nuclide. In these cases, the points on the curved part of the curve were not used in making the machine fit, but were used to try to estimate the half-life of the parent nuclide.

5.2. Coincident β-Transition Energy Measurement

To roughly formulate a decay mode for a newly investigated nuclide, we had to determine the Q value of the β decay of each of the unknown γ lines. Therefore we had to record the β spectrum coincident to the γ line and, in a subsequent step, check whether the γ line was not part of a γ-γ cascade. β ground-state transitions possibly occurring in the decay mode cannot be detected by this method.

The detector system and electronic equipment for recording such β spectra two-dimensionally in triple coincidence of Ge diode, β-transmission counter, and β-anthracene crystal, are described in Secs. 3.3 and 3.4.

The multichannel analyzer was divided into a matrix of 16 x 256 channels. Sixteen channels in the γ-direction were enough to register the sharp γ line supplied by the Ge detector; the portion of the total γ spectrum containing the line was selected by an input format selector. Two hundred and fifty six channels were available in the β-direction. The position of the γ line and its background within the 16 channels was first exactly determined in the γ-direction by one-dimensionally observed, but pseudo-two-dimensionally registered measurement. The true two-dimensional spectrum was then recorded. An example is shown in Fig. 8. The measurement intervals were of the same order of magnitude as those reported in Sec. 5.1.

Out of each 16 β spectra, those containing the photopeak of the γ line under investigation were added together for evaluation. A mean spectrum was formed from the adjacent β spectra on both sides, and deducted from this summary spectrum. Thus we could truly deduct the coincident background beneath the photopeak of each γ line. This is possible only for two-dimensional registration of the β-γ spectra. It would not be possible if the γ-coincident β spectra were recorded one-dimensionally by controlling the multichannel analyzer gate by means of the coincidence signal of a single-channel discriminator adjusted to the photopeak.

To determine maximum β energy, we subjected the β spectra obtained by addition and deduction of background to Fermi-Kurie analysis. The results are shown in the figures in Sec. 7. Some of the statistical errors in the curves are large because the integrated photopeak intensity detected by the Ge diode is only moderate for coincidence tests. We determined the point of intersection of the Fermi-Kurie line with the energy axis, i.e., the peak energy of the spectrum, as follows. Several successive straight lines were drawn through the test points by means of a computer program (weighted least-squares fit) by successively omitting one additional test point from the analysis, starting from the lower energy side. The abscissas of these lines approach a saturation point which determines the β energy.

The lower energy portion of the Fermi-Kurie plots sometimes deviates greatly from the line determined in this manner. This can be attributed to β-particle energy losses in the transport band, in the vacuum window of the measuring chamber, in the β-transmission counter, and in the anthracene crystal cover. However, in some cases it also involves superposition of the desired β spectrum over a lower energy β spectrum belonging to another coincident γ line. We made no attempt to resolve the spectrum into several components because of inadequate statistical data for the curves.

To eliminate correcting for the β-particle energy losses mentioned above, and to avoid the possibility of contamination of open β-calibration specimens, we calibrated the β-spectrometer energy with known, long-lived fission products. Bρ values and cycle duration were in each instance adjusted to the optimum for the nuclides ^{85m}Kr,

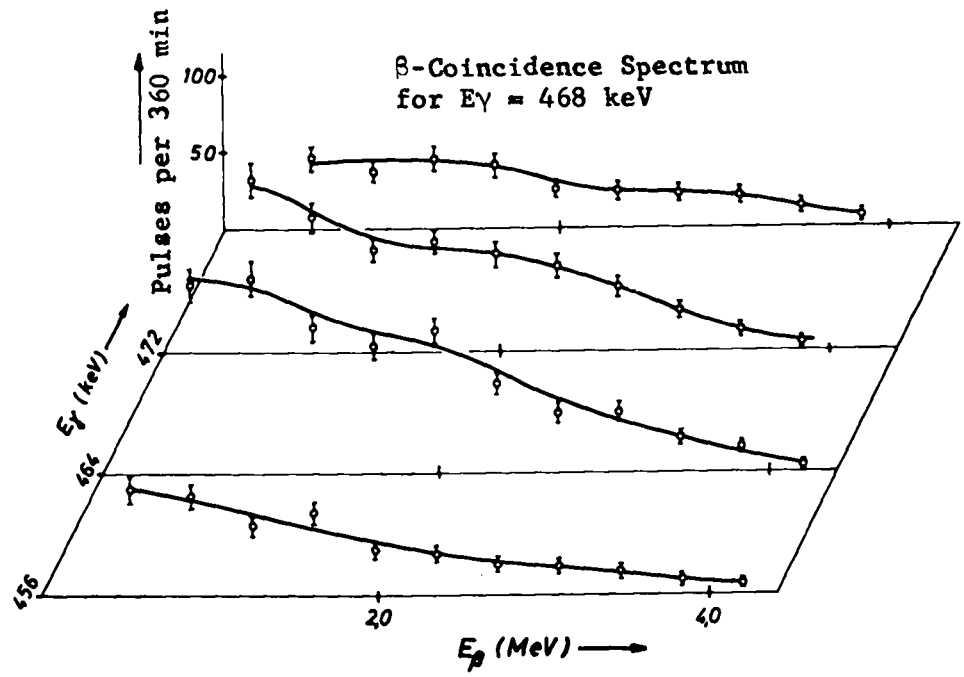

Fig. 8. Example of a two-dimensional β-γ spectrum.

^{101}Tc, ^{94}Sr, ^{88}Kr, ^{87}Kr, and ^{90}Rb. The coincident β energies for the strong γ lines of these nuclides (see Table I, Sec. 4.2) were taken from Refs. 11 and 18. The channel number corresponding to peak energy was found from the Fermi-Kurie plots in the manner described above. The calibration line is shown in Fig. 9.

5.3. Check for γ-γ Cascades

When the energy of a β transition coincident to a γ line has been determined, the sum of γ and β energy yields the Q value of β decay only if the γ line is not part of a γ-γ cascade. Therefore, we also had to determine the γ-γ coincidence spectrum for each of the 12 new γ lines investigated. For this purpose we replaced the anthracene crystal by a 3-in.-diam, 5-in.-long NaI crystal operated in coincidence with the β-transmission counter and the Ge diode. With the geometry used, the NaI crystal had a detection probability of $1.5 \cdot 10^{-2}$ for a γ energy of 1330 keV. To keep the background from incident β particles low, the crystal was shielded by a 6-mm-thick aluminum absorber plate which absorbed β energies up to 3 MeV. The γ spectrum coincident to the γ line under investigation was obtained two-dimensionally like the β spectra described in Sec. 5.2. Figure 10 shows a typical example. Several single spectra were added, and the coincident background was subtracted as in Sec. 5.2. The final γ-γ coincidence spectra thus obtained are given in Sec. 7 with the descriptions of the new nuclides investigated.

Since the detection probabilities of both the Ge detector and the NaI crystal are absolutely calibrated, it is possible to indicate the relative intensity of coincident γ lines found. How-

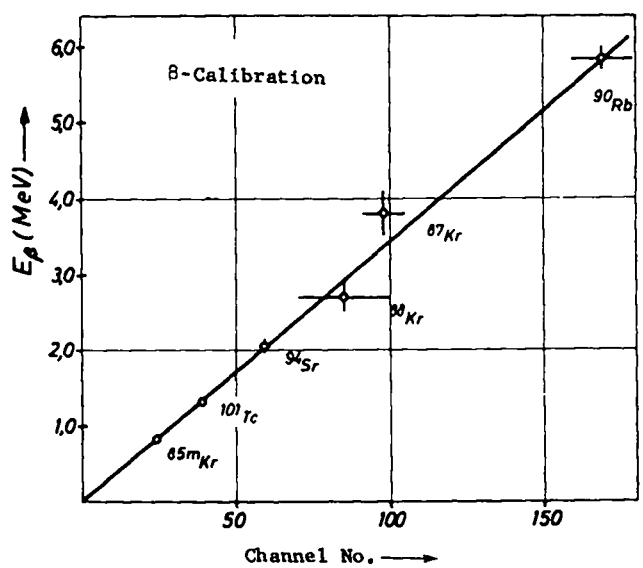

Fig. 9. Energy calibration of the β-scintillation spectrometer.

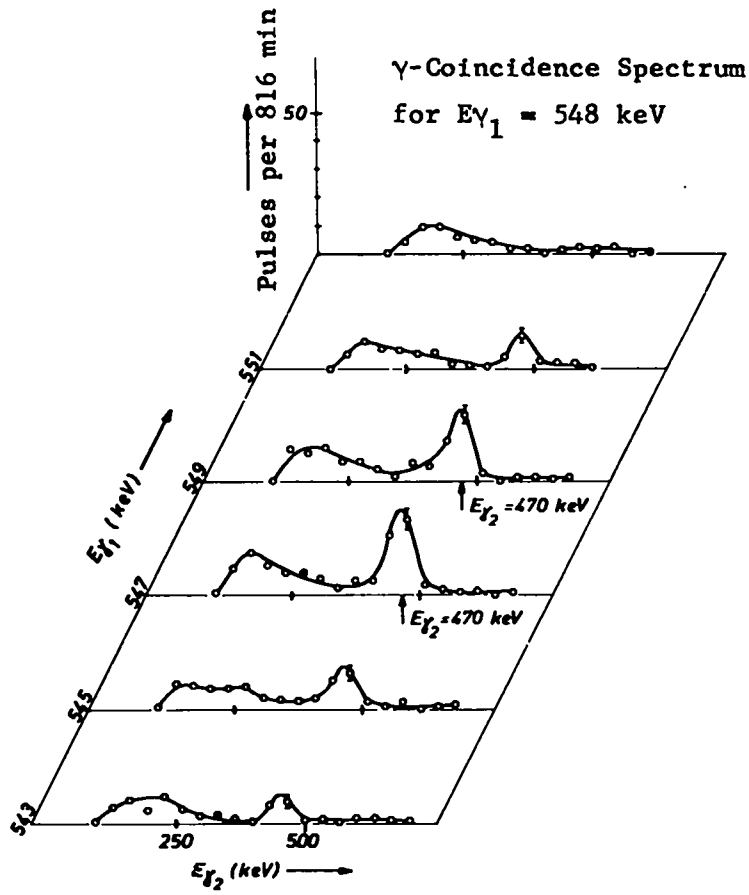

Fig. 10. Example of two-dimensional γ-γ spectrum.

ever, this determination can only be rough, because the statistics for the γ-coincidence spectra are only fair due to lack of intensity, as in the case of the β-coincidence spectra.

With the low intensity and moderate resolving power of the NaI crystal, it is difficult to separate several energetically adjacent lines. If a coincident γ line is present, the lower energy portion of the spectrum cannot be further evaluated for additional coincident lines. A background of events builds up in which the coincident γ rays are Compton-scattered either in the NaI crystal or in the surrounding matter. Below 150 keV, the spectra are unfortunately limited by a threshold in the two-dimensional electronic array. Coincident γ lines of very low energy may therefore be overlooked. However, their contribution to the decay Q value would be smaller than the error in β-energy measurement.

6. CORRELATION OF TEST DATA

6.1. Correlation Criteria

The measurements described in Sec. 5 provided the following results for the 12 unknown lines: half-life, coincident β-transition energies, and detection of possible coincidence of the lines with each other or with other lines not detected in the test runs. From γ-γ coincidence measurement, several pairs from the 12 lines could immediately be recognized as belonging to the same nuclides.

We considered all available criteria in identifying the new nuclides. The mass value defined by the Bρ position of the line provided the decisive indication for correlation. Where primary nuclides were considered in correlation, we had to compute their apparent mass shift according to the equations and numerical values given in Sec. 2.4.

The half-life measurements provided additional arguments. In several instances, the assigned half-

life of the nuclide was already known from radiochemical measurements. In other instances, the activity curve showed a buildup from the parent nuclide during the first moments after irradiation; it follows therefrom that the parent nuclide must have a cumulative yield and half-life comparable to the nuclide under consideration.

Another indication of the identity of the nuclide in a mass chain could be obtained from the measured γ-line's intensity. With absolute calibration of the Ge-diode detection probability, and computation of the transport band time yield function, we could roughly estimate the line yield and compare it with the cumulative yield of the nuclide in question. The cumulative yield of the nuclide may be larger than the line yield when the nuclide's γ line falls together with a second γ transition or with the β ground-state transition that cannot be detected.

In several instances, we found data for (n,γ) or (d,p) reactions in stable nuclei on the energy levels excited in the outer nuclei of nuclides that might possibly be affected.

The Q value measured as a sum of β and γ energy was considered an important criterion for correct assignment. The experimental value must fit easily into the Q-value system. For this purpose, we drew Way-Wood lines from the known Q values for the mass range A = 78 to 106. These are shown in Figs. 11 through 14. The Q values of newly investigated, correlated nuclides and the respective errors are shown in these figures.

Using the criteria mentioned, we compared the measured data with a list of candidates containing nuclides with unknown decay modes and isomeric states of already known nuclides in the respective mass range. Applying all criteria and considering test errors left only one candidate for correlation for each γ line or for each γ-γ cascade recognized as being coincident. In two cases several lines had to be attributed to the same nuclide although they had not been observed in coincidence.

6.2. Summary of Identified Nuclides

The 12 new γ lines investigated and reported in Sec. 4.4 were identified as lines of the following eight nuclides.

^{84}Se, ^{91}Kr, ^{97}Y, ^{99}Nb,
^{99}Zr, ^{100}Nb, ^{101}Nb, ^{101}Zr.

The identified nuclides are discussed in detail in Sec. 7.

In three cases it was impossible to estimate the as yet unknown half-life of the parent nuclides. These were ^{97}Sr, ^{99}Y, and ^{100}Zr.

Figure 15 shows a section of the nuclide chart for the light fission-product range. The eight identified nuclides for which we arrived at a decay mode, and the three whose half-lives we could estimate are indicated by heavy squares. The half-lives of known nuclides were taken from Refs. 18 and 28. The following data were used in modification or in addition: del Marmol's values[29] for ^{83}As and ^{84}As; del Marmol and Neve de Mevergnies' data[30] for ^{85}As and ^{87}As; Tomlinson's data[31] for ^{87}Se; the results of Amarel et al.[32] for the rubidium isotopes 90 through 96 and the strontium isotopes 95 and 96; Gauvin's data[32a] for ^{97}Rb; Patzelt and Herrmann's values[33] for the krypton isotopes 92 through 94; and, finally, the results of Huebenthal et al.[34] for ^{98}Zr and ^{98}Nb. The fission yields for individual mass chains were taken from Ref. 28. The centroid Z_p as computed from the data reported in Sec. 2.4 is shown in Fig. 15 to illustrate the primary nuclear charge distribution within a chain.

7. DISCUSSION OF IDENTIFIED NUCLIDES

7.1. Selenium-84

The 406 ± 3-keV line (see Table III, Sec. 4.4) could be attributed to ^{84}Se. The half-life of this nuclide was known and was last determined by Sattizahn et al.[35] as 3.3 ± 0.3 min. Sattizahn separated selenium from a fission-product mix by a rapid chemical method, successively extracted the bromium formed, and then measured the ^{84}Br activity (milking method).

The Bρ position at which the 406-keV line was found corresponds to a mass value of 84.2 ± 0.2. The theoretical ^{84}Se mass to be expected at the mass separator is 84.0; i.e., there is no apparent mass shift. Although the nuclide may also be primary, dA (see Eq. (16), Sec. 2.4) remains approximately zero because Γ in this range is close to 1.

Figure 16(a) shows the half-life measurement for the 406-keV line. The obtained value is 3.5 ± 0.1 min which agrees well with Sattizahn's earlier value. Del Marmol[29] reported the half-life of the parent nuclide, ^{84}As, as 5.8 sec. It

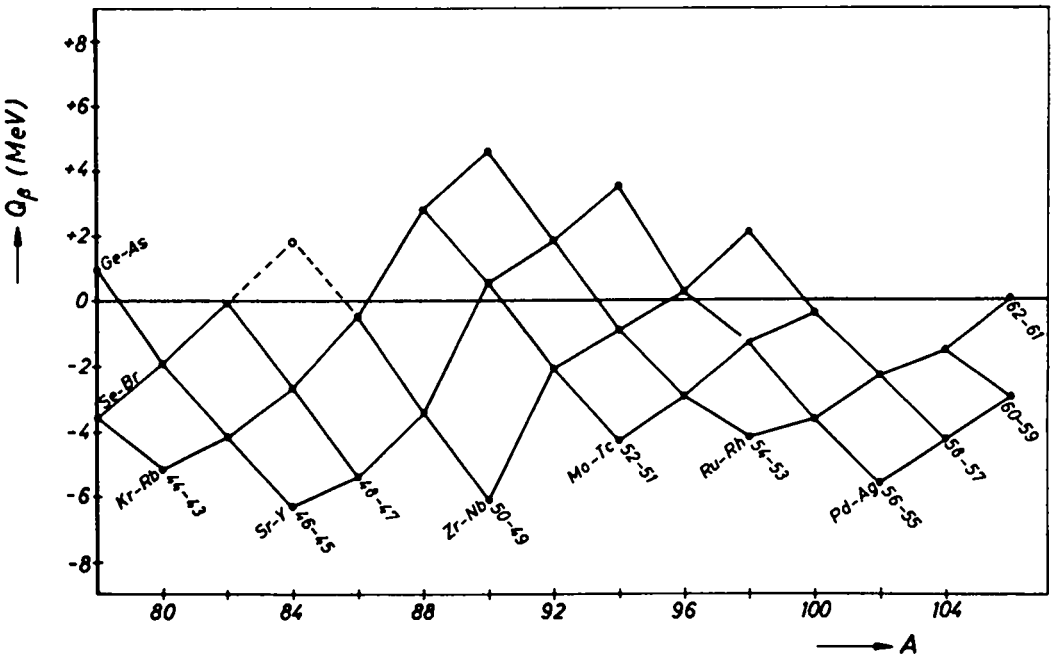

Fig. 11. Way-Wood lines for even-even nuclei.

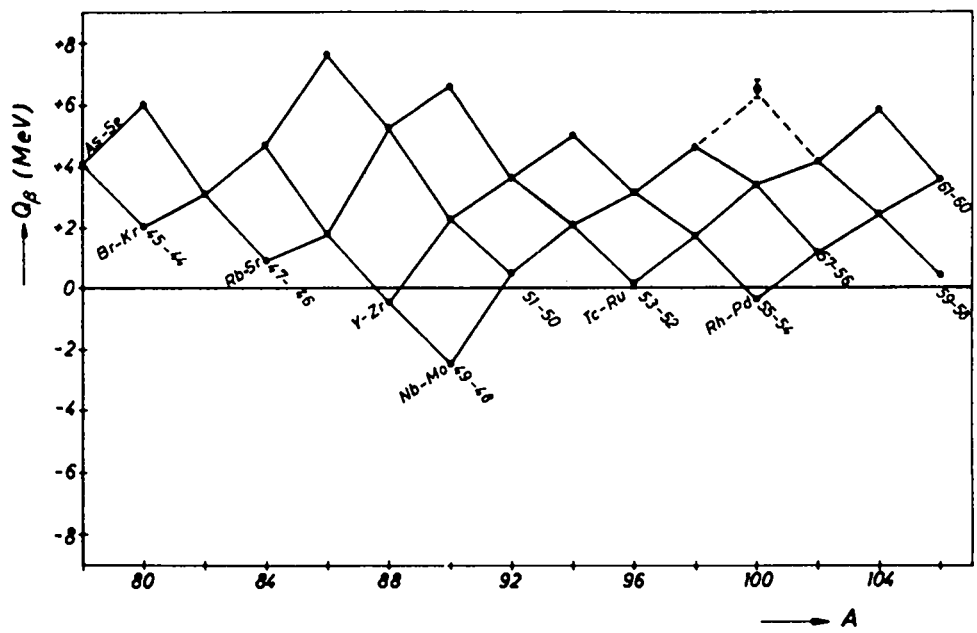

Fig. 12. Way-Wood lines for odd-odd nuclei.

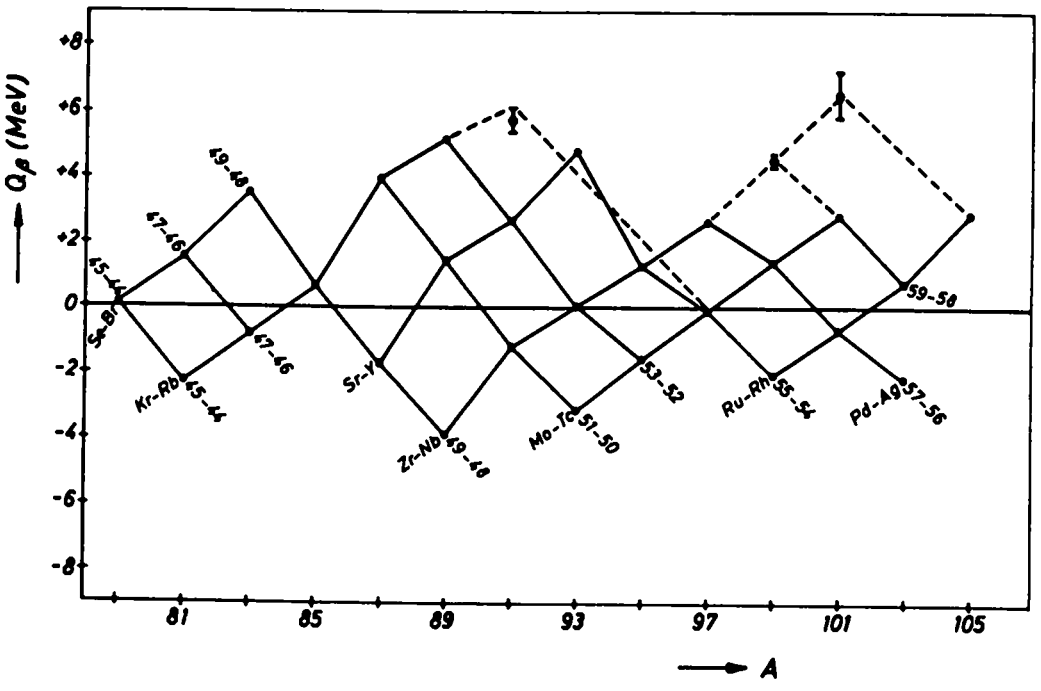

Fig. 13. Way-Wood lines for even-odd nuclei.

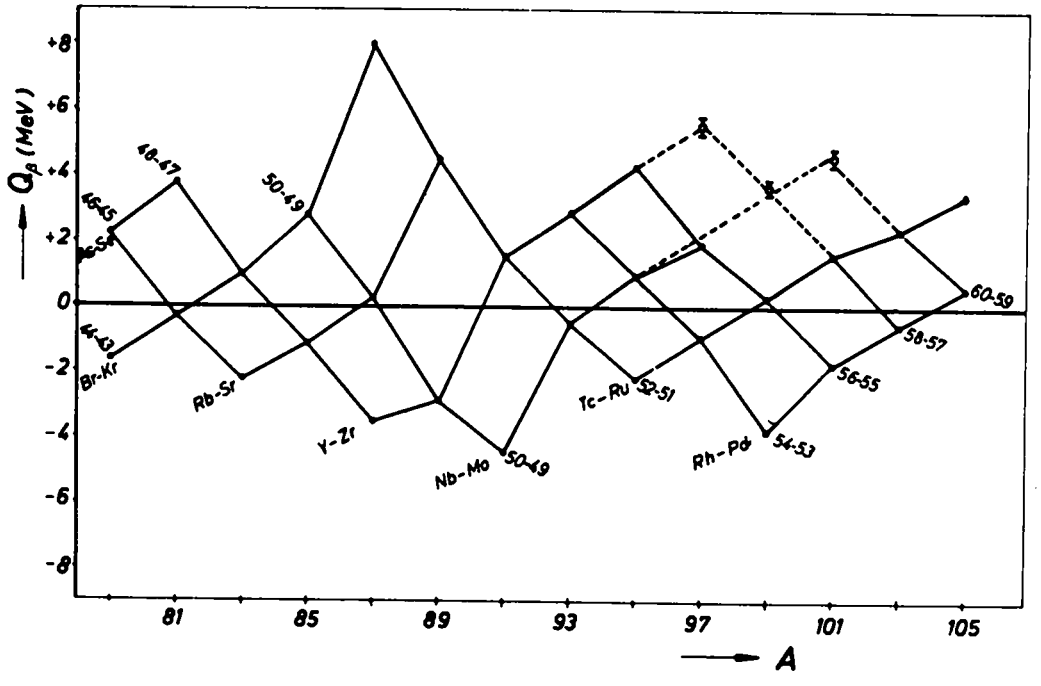

Fig. 14. Way-Wood lines for odd-even nuclei.

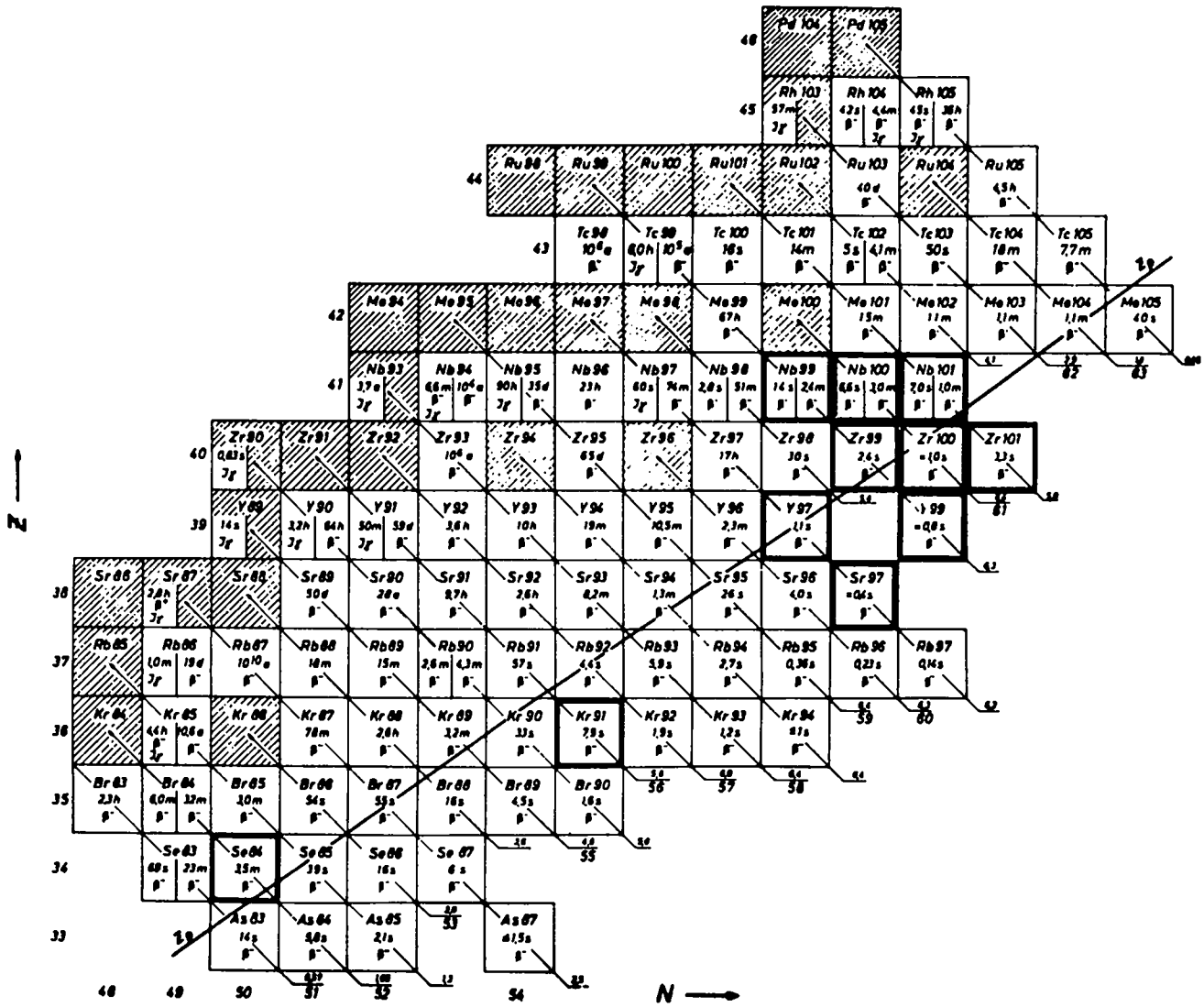

Fig. 15. Section of the nuclide chart for the light fission-product range.

is compatible with these data that activity decay shows no curvature at the beginning of the line in a semilogarithmic plot.

Fermi-Kurie analysis of the coincident β transition, Fig. 16(b), yields a β energy of 1.4 ± 0.1 MeV. The γ-γ coincidence spectrum, Fig. 16(c), shows no γ line coincident to 406 keV. Thus the decay Q value is 1.8 ± 0.1 MeV which fits well into the Way-Wood diagram for even-even nuclei (Fig. 11).

Using the values for primary nuclear charge, Z_p, introduced in Sec. 2.4 and shown in Fig. 15, one obtains a cumulative yield for ^{84}Se of about 90% of the chain yield. Using the 406-keV line intensity and considering the transport-band time functions, one can estimate a γ-transition yield of the same magnitude as the chain yield. Accordingly, practically 100% of the ^{84}Se decay occurs above the 406-keV line. Since we did not observe strong γ-γ coincidences to 406 keV, we assumed this same yield for the 1.4-MeV β transition. Using the half-life, we then computed the value of log ft as about 4.0, which amounts to an allowed transition.

From these results, we show a proposal for an ^{84}Se decay mode in Fig. 17. Sattizahn[35] had shown that, within the accuracy of measurement, ^{84}Se decays only to 32-min ^{84}Br, not to 6-min

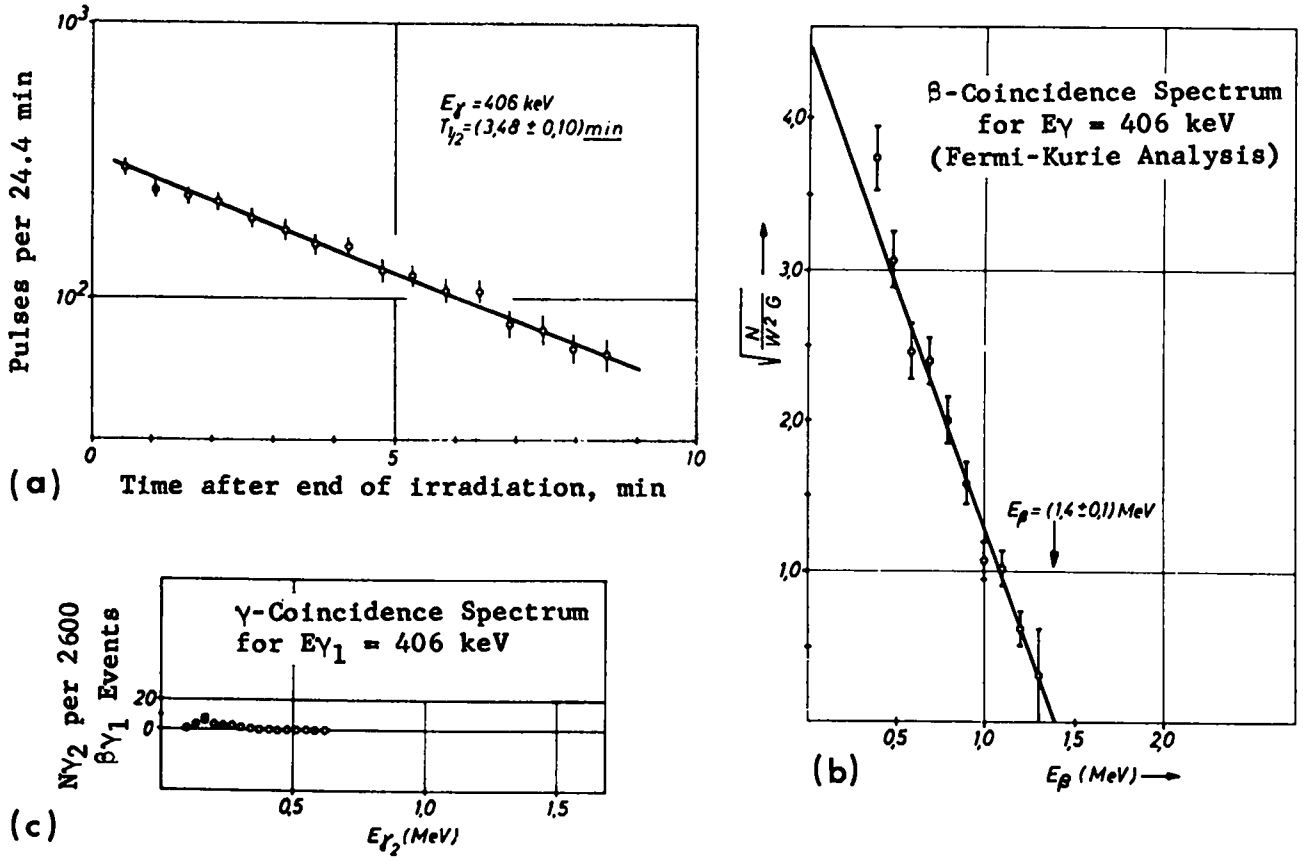

Fig. 16. (a) Decay curve, (b) β-coincidence spectrum, and (c) γ-coincidence spectrum for the 406-keV line of ^{84}Se.

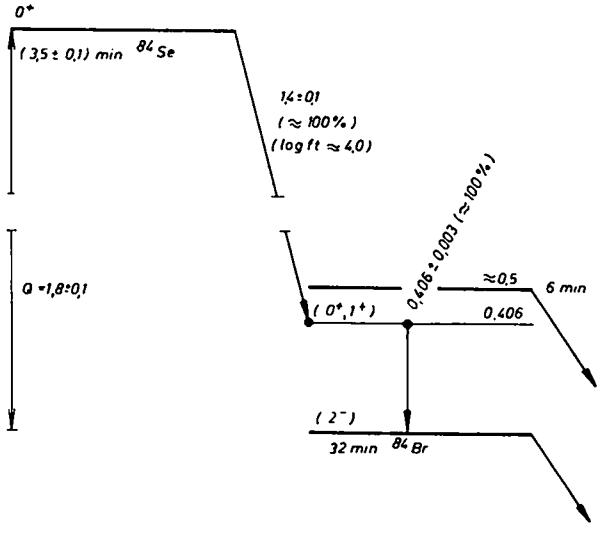

Fig. 17. Proposed ^{84}Se decay mode.

^{84}Br. Although Sattizahn states that he could not establish the energy position of the 6-min isomer he discovered, it is given in Ref. 18 without additional references as about 0.5 MeV above the 32-min ground state. We adopted this value for Fig. 17.

As an even-even nucleus, ^{84}Se in the ground state has 0^+ spin and parity. Since the β transition is allowed, the excitation level of the daughter nucleus, ^{84}Br, can only have 0^+ or 1^+. Reference 18 reports 1^+ or 2^- for the 32-min ground state. Accordingly, for 1^+, the β ground-state transition from ^{84}Se to ^{84}Br must also be allowed, but the high yield of the 406-keV line stands against this possibility. Therefore the ^{84}Br ground state is assigned 2^-. Examination of the unstable even-even nuclei ^{78}Ge, ^{88}Kr, and ^{90}Kr in the vicinity of ^{84}Se indicates that the β decay there also leads to ground states of the daughter nuclei with 2^- spin and parity.

According to the assignments made, the 406-keV radiation is accompanied by a change of parity. The level lifetime is shorter that the 0.2-μsec coincidence resolution only in the case of an E1 or M2 transition, so the line can be observed in β-γ coincidence.

7.2. Krypton-91

The 111 ± 3-keV γ line reported in Table III was attributed to ^{91}Kr. The half-life of this nuclide has long been known as about 10 sec. Gamma spectroscopy was last reported by Amiel et al.[36] They separated the inert gases krypton and xenon from a fission-product source by a gas-flux method. There they found a 108-keV line with a half-life of 8.5 ± 1.5 sec and a three times weaker 509-keV line with a half-life of 8.5 ± 3 sec. Borg et al.,[37] who introduced the gas flux into the ion source of an isotope separator, had earlier attributed a 109.2-keV line to the mass chain 91.

The Bρ value of the 111-keV line and the mass-calibration curve show a mass value of 90.9 ± 0.3. By using the derivations in Sec. 2.4, one obtains a theoretical value of A_{sep} = 91.5 ± 0.2 for ^{91}Kr, based on the values and estimated errors for ΔZ.

For purely accidental experimental reasons, the decay curve, Fig. 18(a), is available only in the form of rough half-life analysis for which the measuring interval was divided into four subgroups. Computer fit yields a half-life of 7.9 ± 0.5 sec which agrees with Amiel's value within the limits of error. Because of the coarse time grid, we cannot determine the lifetime of the parent nuclide of ^{91}Kr.

Figure 18(b) shows the β-coincidence spectrum for the 111-keV line in the form of a Fermi-Kurie plot. Analysis yields a β energy of 5.5 ± 0.4 MeV. The γ spectrum coincident to 111 keV, Fig. 18(c), contains a 630 ± 20-keV γ line with a yield about one-eighth that of the 111-keV line. The lower intensity γ line must be the upper line of the γ-γ cascade. Amiel's 509-keV line was not found in the special β-γ-γ spectrum or in the β-γ spectra of the test runs.

Using the Z_p data from Sec. 2.4, we estimate the cumulative yield of ^{91}Kr to be about 40% of the chain yield. The yield computed from the intensity of the 111-keV line is about 30% of the chain yield. Accordingly, about 80% of the ^{91}Kr decay events follow the 111-keV line. Seven eighths of this energy level is then occupied by direct β transition, and one eighth by lower energy β transitions utilizing the higher 630-keV γ transition. The β-coincidence spectrum for 111 keV is therefore shifted somewhat to lower energy values. This effect is estimated at about 0.1 MeV. Thus the coincident β energy is 5.6 ± 0.4 MeV. The decay Q value is then 5.7 ± 0.4 MeV, which fits fairly well into the Way-Wood diagram for even-odd nuclei (Fig. 13).

Assuming a 70% branching ratio for the transition, log ft for the 5.6-MeV β transition is 5.3 which is still within the range of allowed transition values.

The test results are summarized in a proposed mode of ^{91}Kr decay (Fig. 19). For the daughter nucleus, ^{91}Rb, Kofoed-Hansen and Nielsen[38] stipulated a 14-min isomer in addition to the 1-min ground state. However, neither Wahl et al.[39] nor Wahlgren and Meinke[23] and Amarel et al.[32] observed a 14-min ^{91}Rb activity, so only the ground state is confirmed by experiment. The value given in Ref. 32 is adopted as the latest half-life measurement.

According to the shell model, five $d_{5/2}$-neutrons combine to a $5/2^+$ state for the ^{91}Kr ground state. The same spin and parity values are given in the literature for the neighboring even-odd nuclei, ^{87}Kr, ^{89}Kr, ^{91}Sr, ^{93}Sr, and ^{95}Zr. For the odd-even nuclei among the rubidium isotopes, the ground state is defined by either $p_{3/2}$- or $f_{5/2}$-protons, depending on the number of neutrons. Comparison with neighboring odd-even nuclei of the same neutron number as ^{91}Rb is not possible because the $p_{3/2}$ and $f_{5/2}$ subshells are already completely filled, and higher subshells are being occupied. Accordingly, for the ^{91}Rb ground state, we cannot decide between $3/2^-$ and $5/2^-$. Since β transition to the 111-keV energy level is permitted, it may have $3/2^+$, $5/2^+$, or $7/2^+$.

The parity-modifying 111-keV radiation can be only of the E1 type. The lifetime of the energy level corresponding to M2 radiation is already about 10^{-4} sec. In this case, one could not detect the line in the β-γ coincidence circuit because of the 0.2-μsec resolution time.

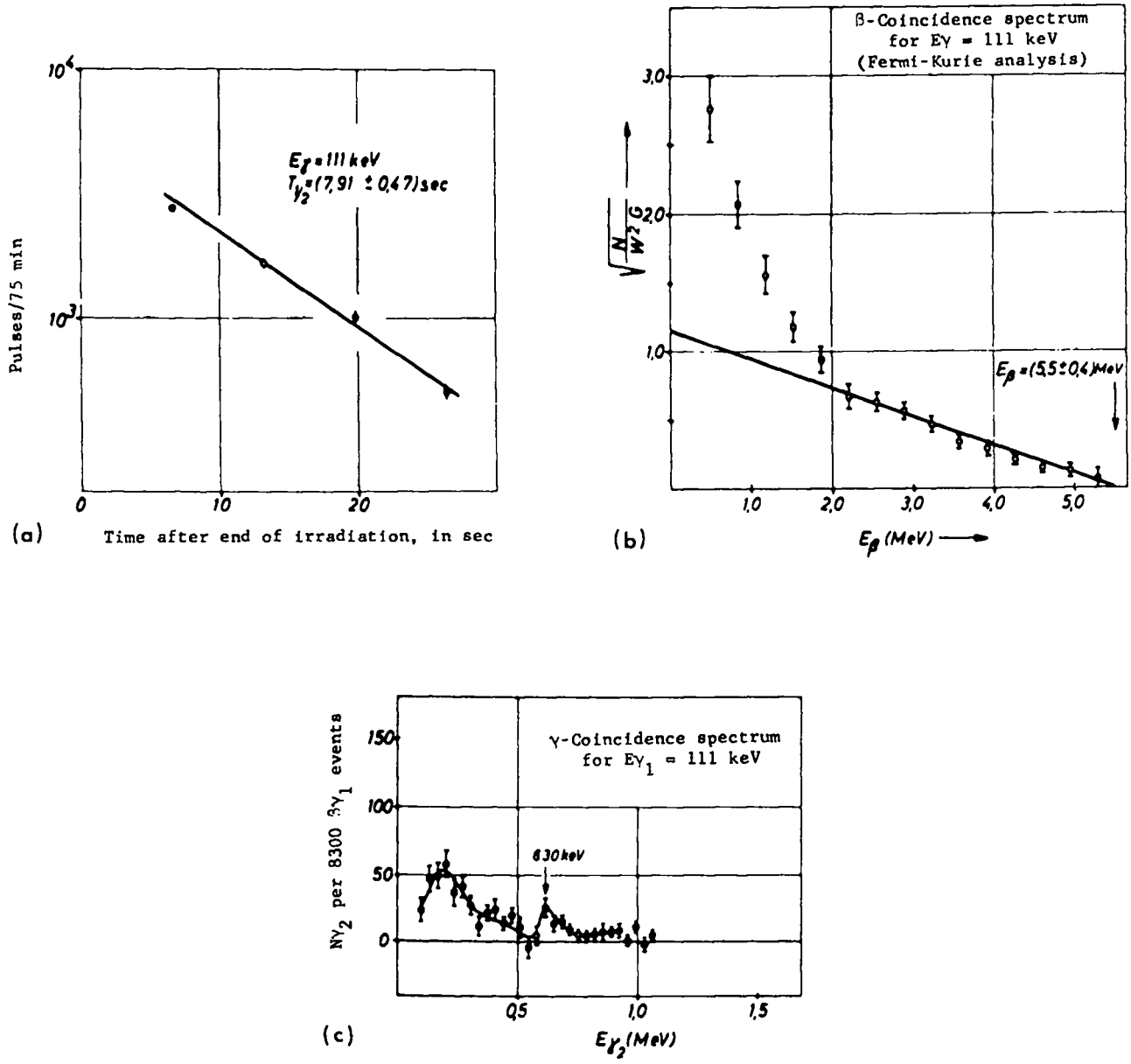

Fig. 18. Decay curve, β-coincidence spectrum, and γ-coincidence spectrum for the 111-keV line of ^{91}Kr.

7.3. Yttrium-97

During γ-γ measurements, we recognized two of the new γ lines, the 125 ± 3-keV and 810 ± 3-keV lines, as being coincident. They could be attributed to ^{97}Y. To date, only one half-life determination, by Niece,[40,41] is available for this nuclide. Starting with a fission-product mix, he determined the independent yield of ^{97}Zr as a function of time, and on this basis estimated the ^{97}Y half-life to be 6 ± 2 sec.

The experimental mass values implied by the Bρ location are 97.6 ± 0.3 for the 125-keV line and 96.6 ± 0.7 for the 810-keV line, or an average of 97.3 ± 0.3. The theoretical ^{97}Y value which takes into account the apparent separator mass shift is 97.6 ± 0.3.

Figure 20(a) shows the time decay of the two lines in a semilogarithmic plot. The half-lives are 1.11 ± 0.03 sec for the 125-keV line and 1.09 ± 0.07 sec for the 810-keV line, or an average of 1.11 ± 0.03 sec. Niece's value agrees with the latter only by order of magnitude. Niece's method

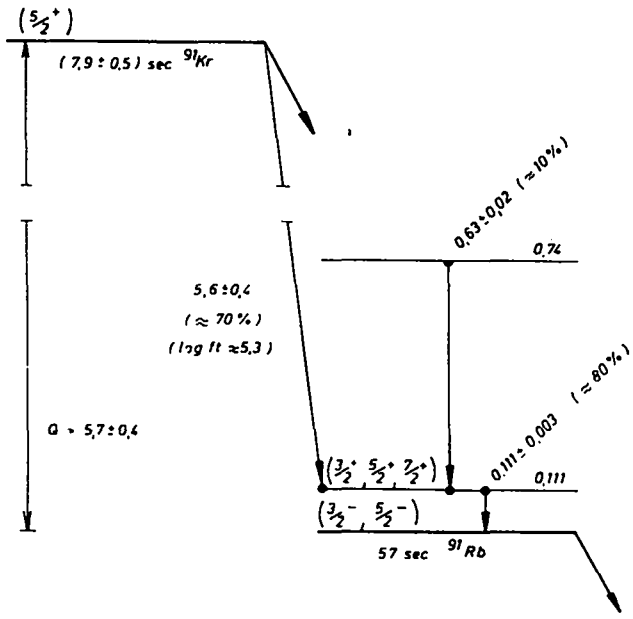

Fig. 19. Proposed ^{91}Kr decay mode.

may possibly be affected by the fact that the jump in half-life from ^{97}Zr to ^{97}Y is more than four orders of magnitude.

With our assumption about the Z_p distribution, we can estimate the primary yield of ^{97}Y to be about 60%, and the cumulative yield of the parent nuclide, ^{97}Sr, to be about 20%, of the chain yield. With this ratio of birth rates, the fact that the activity curves in Fig. 20(a) do not show any appreciable buildup at the selected irradiation time suggests an estimated 0.4 ± 0.3 sec for the ^{97}Sr half-life.

Figures 20(b) and (c) show the Fermi-Kurie analysis of the β-coincidence spectra for the two γ lines. Evaluation yields coincident β energies of 4.9 ± 0.2 and 4.6 ± 0.3 MeV for the 125- and 810-keV lines, respectively. Figure 20(d) shows the 125-keV γ- coincidence spectrum in which the 810-keV line is pronounced. Conversely, the 125-keV line no longer appears in the 810-keV γ-coincidence spectrum, Fig. 20(e), because it falls below the electronic threshold mentioned in Sec. 5.3.

From the 125- and 810-keV line intensities, we computed that, within experimental accuracy, both yields approximately equal the chain yield, with the 810-keV line apparently having a somewhat smaller yield. The cumulative ^{97}Y yield is about 80% of the chain yield. Accordingly, almost all of the ^{97}Y decay events follow the γ-γ cascade. From the fact that both γ lines have nearly equal yield, and that the respective coincident β energies agree within the limits of error, one may conclude that it is essentially the higher, rather than the middle, energy level which is being filled by β decay. From this conclusion, the β energy is averaged from the two measurements as 4.8 ± 0.2 MeV. By adding the γ-γ cascade energy, we obtain a Q of 5.7 ± 0.2 MeV which fits well into the system of Way-Wood lines for the odd-even nuclei (Fig. 14). The log ft of the β transition is about 4.1, which amounts to an allowed transition.

Figure 21 shows a proposed ^{97}Y decay mode. For the ground state of the daughter nucleus, ^{97}Zr, Cohen[42] measured $1/2^+$ spin and parity by the ^{96}Zr(d,p) reaction. A value of $7/2^+$ would have been expected from the shell model. In a second study, Cohen and Chubinsky[43] also determined ^{97}Zr excited levels by the same method. The lowest states found were a $3/2^+$ state for 1110 keV and a $7/2^+$ state for 1270 keV. It is striking that 1110 and 810 keV, as well as 1270 and 935 keV (= 810 keV + 125 keV), differ by a constant factor of 1.37 to 1.36. But it is unreasonable to assume such a deviation in the energy calibration factor for the (d,p) measurements.[43] For instance, both Larson and Gordon's[44] investigation of ^{95}Y β decay and that by van Klinken et al.[45] agreed well with the levels found in Ref. 43 using the ^{94}Zr(d,p) reaction. Since Cohen and Chubinsky pointed out that they had particularly great difficulty with contamination from ^{96}Zr(d,p) reaction, we concluded that the states filled by β decay are, in fact, located below the 1110-keV energy level. In the (d,p) measurement, these states are easily hidden by interference when excitation occurs with only a moderate excitation cross section.

The sequence of the two γ lines in the γ-γ cascade is at first uncertain. However, although the lower values of the 810-keV line are within the limits of error, the higher yield and coincident β energy of the 125-keV line is considered an indication that the 125-keV line is the lower line in the cascade. The light shift of yield and β energy would then be caused by low direct population of the middle level of the cascade.

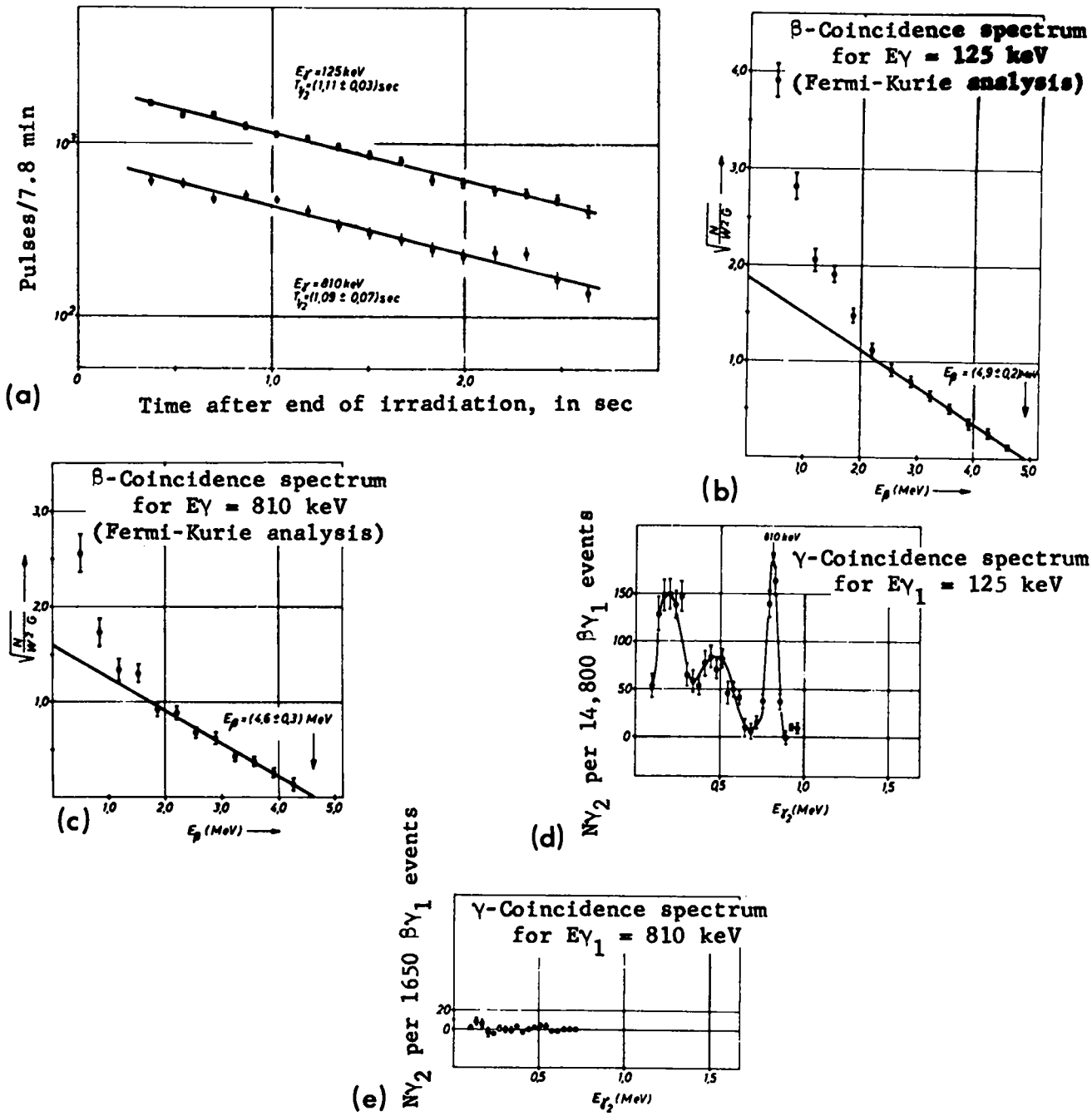

Fig. 20. Decay curves, β-coincidence spectra, and γ-coincidence spectra for the 125- and 810-keV lines of ^{97}Y.

The $1/2^-$ spin and parity implied by the shell model is assumed to be the ^{97}Y ground state, as is partially confirmed by experiment on neighboring yttrium isotopes with even neutron number. Then the allowed β transition can lead only to a $1/2^-$ or $3/2^-$ level. These spin and parity values show also, when the assumption about the ^{97}Y ground state is accepted as correct, that the energy levels filled by β decay cannot be identical with those found by Cohen and Chubinsky.

7.4. Niobium-99

The 137 ± 3-keV line was attributed to ^{99}Nb. The ground state and one isomeric state are known for this nuclide. The longer-lived state (2.5 min) was first observed by Duffield et al.[46] after a ^{100}Mo(γ,p) reaction. Orth and Smith[47] measured a

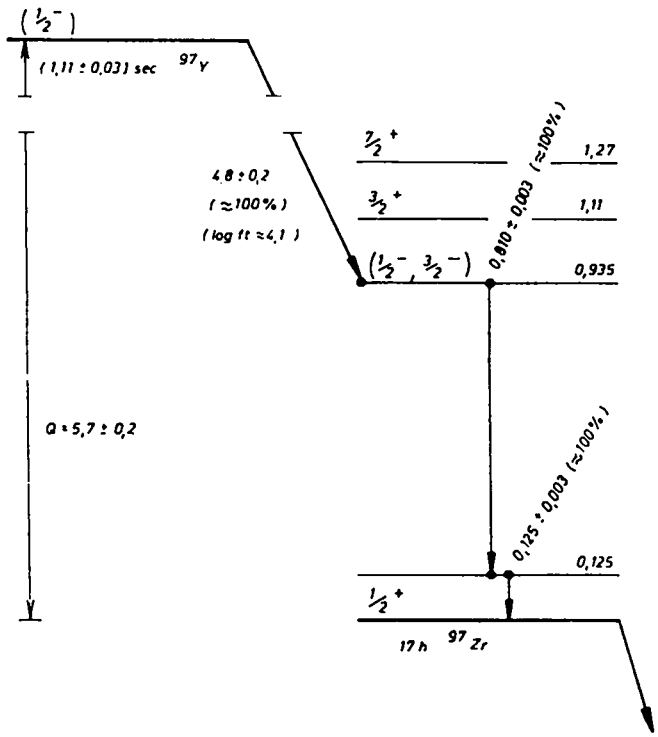

Fig. 21. Proposed ^{97}Y decay mode.

half-life of 2.4 ± 0.3 min for fission products and substantiated two γ lines of 100 and 260 keV. Among the fission products, Troutner et al.[48] found, in addition to a 2.3-min state, a shorter-lived state with a half-life of 10 ± 2 sec which must decay directly into the daughter nucleus, ^{99}Mo, in at least half of the decay events, whereas a maximum of 36% of the decay events in the chain may take place through the longer-lived state. Huebenthal[49,50] produced the nuclide with the reaction ^{100}Mo(n,np) ^{99}Nb. Here he was unable to observe the longer-lived state. He attributed two γ lines of 98 and 140 keV to the short-lived state for which he determined a half-life of 9 ± 2 sec. However, Kaffrell et al.[51] used the same reaction and found the longer-lived isomer (2.9-min) with γ lines at 97.7, 102.8, and 139.0 keV.

The 137-keV line occurs at a Bρ value corresponding to a mass of 98.8 ± 0.2. The theoretical value is 99.0 since ^{99}Nb is only slightly of primary origin and, therefore, not subject to apparent mass shift.

Half-life analysis of the 137-keV line, Fig. 22(a) yields a value of 14.3 ± 0.6 sec which is somewhat outside the error limits reported by Troutner[48] and Huebenthal.[49,50] An attempt to estimate the half-life of the parent nuclide, ^{99}Zr, from the clear curvature at the beginning of the curve yielded a value of 5 ± 2 sec.

The β energy coincident to the 137-keV line is found from Fermi-Kurie analysis, Fig. 22(b), to be 3.5 ± 0.2 MeV. The γ-γ coincidence spectrum, Fig. 22(c), shows no coincident lines.

From the Z_p values (Sec. 2.4), we compute the cumulative yield of ^{99}Nb to be 100% of chain yield. The intensity of the 137-keV line corresponds to a line yield of the same magnitude as chain yield. It follows that the decay of ^{99}Nb in fission occurs almost exclusively from the 14-sec state. Since the γ line does not coincide with a second line, the β-transition yield is also about 100%. Then log ft will be about 4.5. Accordingly, this is an allowed transition.

To set up the decay mode proposed in Fig. 23, one must further consider the experimental data on excited levels in the daughter nucleus, ^{99}Mo. In the ^{100}Mo(γ,n) reaction, Duffield and Vegors[52] found an isomeric 98-keV level in ^{99}Mo with a half-life of 16 μsec. Hjorth and Cohen[53] investigated the level system by use of the ^{98}Mo(d,p) and ^{100}Mo(d,t) reactions. The lowest excited states are 100 keV with $5/2^+$, 222 keV with $7/2^+$, and 361 keV with $3/2^+$. For the ^{99}Mo ground state, they found $1/2^+$.

From these facts, one must conclude that the 137-keV line fills the isomeric level at 98 keV. In this case, a 98-keV line cannot be observed either in the β-γ or β-γ-γ spectra because the 0.2-μsec coincidence resolving time is small compared to the 16-μsec lifetime. It follows from the energy difference, spin, parity, and lifetime, that the 98-keV line is E2 radiation. The β transition leads to a level at 235 keV (= 98 + 137 keV) which is identified with Hjorth and Cohen's[53] 222-keV level. The 361-keV level they observed would then be emptied by a 260-keV radiation as observed by Orth and Smith[47] in decay of the 2.4-min ^{99}Nb.

The same conclusions are drawn in the decay mode proposed by Huebenthal.[49,50] Furthermore, Huebenthal includes the 44-keV isomer observed by McCarthy et al.[54] This isomer is attributed to ^{99}Mo only because the same lifetime (13 μsec) was measured for the 44-keV isomer and for the known

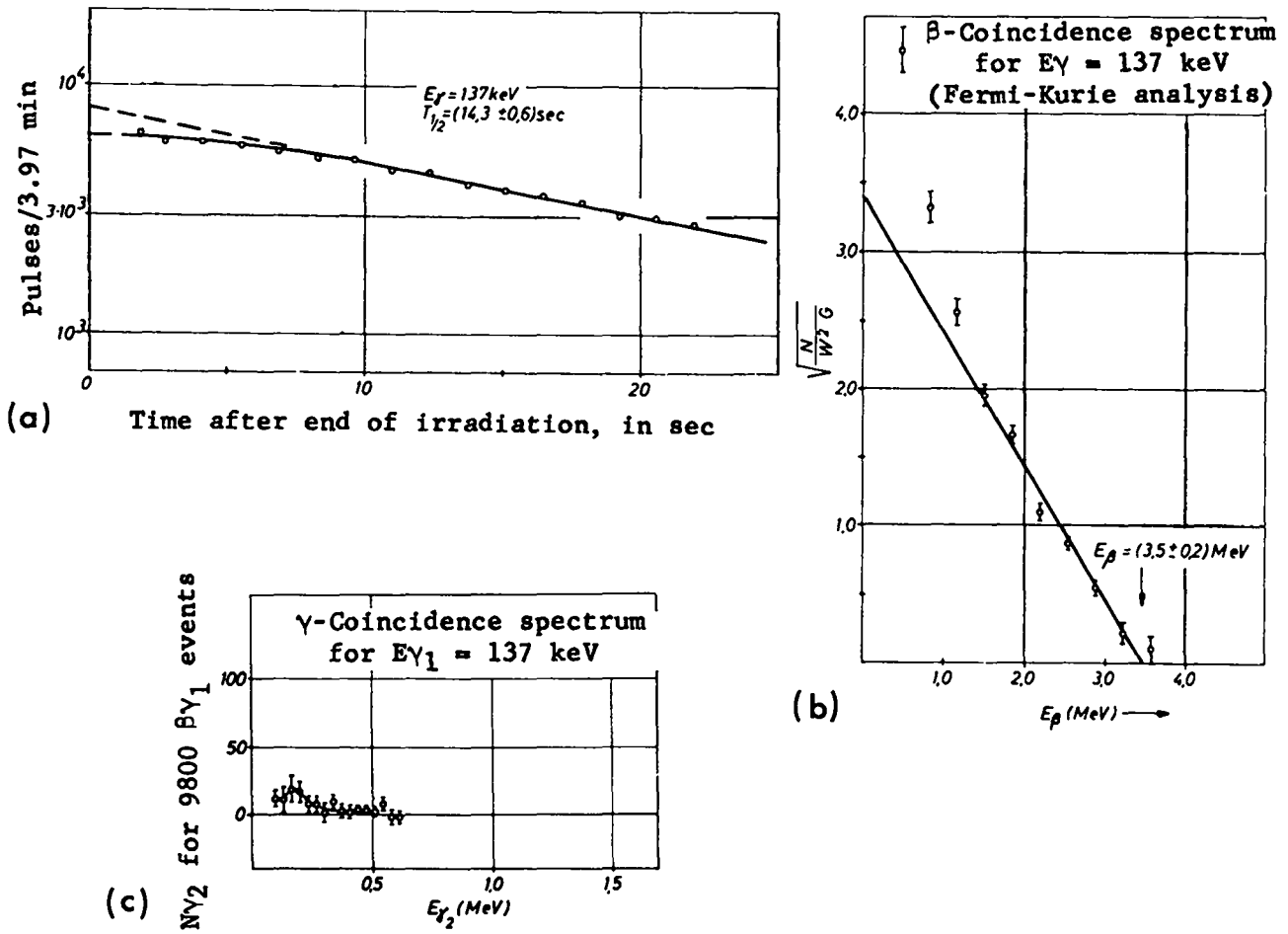

Fig. 22. Decay curve, β-coincidence spectrum, and γ-coincidence spectrum for the 137-keV line of ^{99}Nb.

98-keV isomer of ^{99}Mo.[54] This assignment to ^{99}Mo is not binding because the deuteron beam experiments by McCarthy et al. were performed with a natural isotope mixture of molybdenum. Although Duffield and Vegors,[52] who made the assignment of the 98-keV isomer, also worked with the natural element, they were able to exclude the other molybdenum isotopes on the basis of the threshold energy for production of the isomeric level.

Because of the isomeric state at 98 keV, a total of 235 keV must be added to the 3.5 ± 0.2-MeV β energy measured in coincidence with the 137-keV line to obtain the decay Q value. The 3.7 ± 0.2-MeV Q value fits easily in the Way-Wood diagram for odd-even nuclei (Fig. 14).

Because the 235-keV level is identified with Hjorth and Cohen's 222-keV, $7/2^+$ state,[53] and because of the allowed β decay, only $5/2^+$, $7/2^+$, or $9/2^+$ spin and parity are possible for the 14-sec ^{99}Nb under investigation. The ground state for stable ^{93}Nb was found to be $9/2^+$, and the same configuration was assumed for the ground state of the isotopes ^{95}Nb and ^{97}Nb.[18] According to this system, 14-sec ^{99}Nb has $9/2^+$ spin and parity and represents the ground state decay. All known odd niobium isotopes have isomeric states with shorter lifetimes than the ground state. They are assigned $1/2^-$ spin and parity. The 2.4-min state of ^{99}Nb would then also be assigned the $1/2^-$ configuration. We will maintain the rule that the $1/2^-$ state is located above the $9/2^+$ state as in the other odd isotopes of niobium. However, the high Q-value in this case leads to the ground state decay having a shorter lifetime than the isomer. In emptying

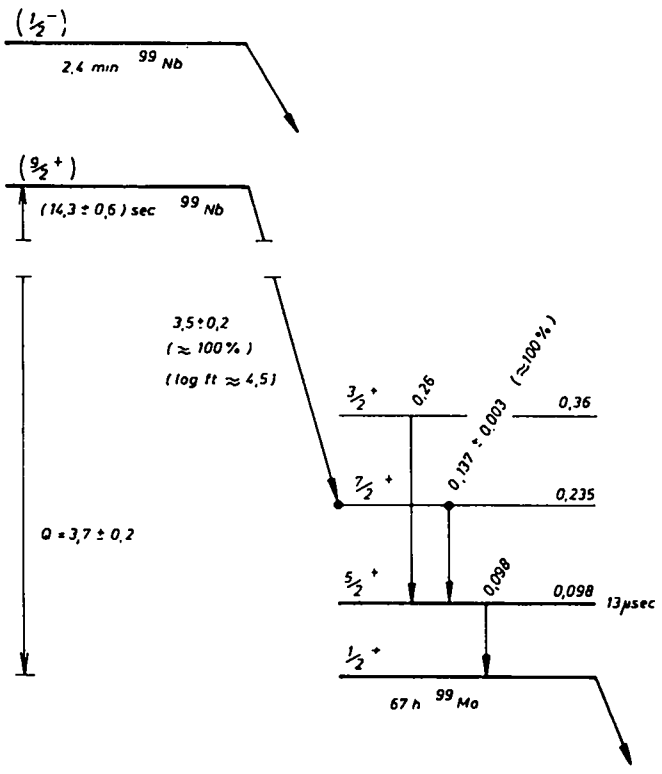

Fig. 23. Proposed ^{99}Nb decay mode.

this isomeric level, an M4 or E5 radiation to the ^{99}Nb ground state competes with a once-prohibited β transition to the 360-keV level in ^{99}Mo. Since the β transition does not seem to have much effect, it follows from the 2.4-min half-life that the isomeric level is several hundred keV above the 14-sec ground state.

7.5. Zirconium-99

In the γ-γ coincidence investigations, the 468 ± 3- and 548 ± 3-keV lines were identified as parts of a cascade. They were assigned to ^{99}Zr. The 595 ± 3-keV line also had to be assigned to the same nuclide. Troutner et al.[48] reported an upper limit of 1.6 sec for the ^{99}Zr half-life. Working with fission products, they investigated the cumulative yield of the amount of ^{99}Mo originating from rapidly separated zirconium as a function of time. They were unable to observe the 35-sec half-life of ^{99}Zr reported by Orth and Smith.[47]

The coincident 468- and 548-keV lines appeared at Bρ positions that lead to masses of 98.6 ± 0.7 or 98.3 ± 1.0, i.e., an average of 98.5 ± 0.6. The mass value of the 595-keV line was 99.0 ± 0.7. Considering apparent mass shift (see Sec. 2.4), the theoretical value for ^{99}Zr is 99.4 ± 0.2.

Figure 24(a) shows the decay curves for the two coincident lines. That the two half-lives, 2.5 ± 0.1 and 2.1 ± 0.1 sec, do not agree within the limits of error may be because one of the lines still contains a small admixture from an adjacent line. The average for the coincident lines is 2.3 ± 0.1 sec. The 595-keV line value, Fig. 25(a), is 2.8 ± 0.3 sec. The average for all three decay curves is 2.4 ± 0.1 sec which agrees with the estimate of Troutner et al.[48]

Both decay curves in Fig. 24(a) seem to have some initial curvature which is hidden in the curve of Fig. 25(a) by the inferior test point statistics. Considering the irradiation time, the half-life of the parent nuclide, ^{99}Y, may thus be estimated as roughly 0.8 ± 0.7 sec. From the assumptions about primary nuclear charges in Sec. 2.4, we assume the cumulative yield of ^{99}Y to be 35%, and the primary yield of ^{99}Zr to be 55%, of chain yield.

The β energy is found from Fermi-Kurie analysis of the respective coincident β spectra as

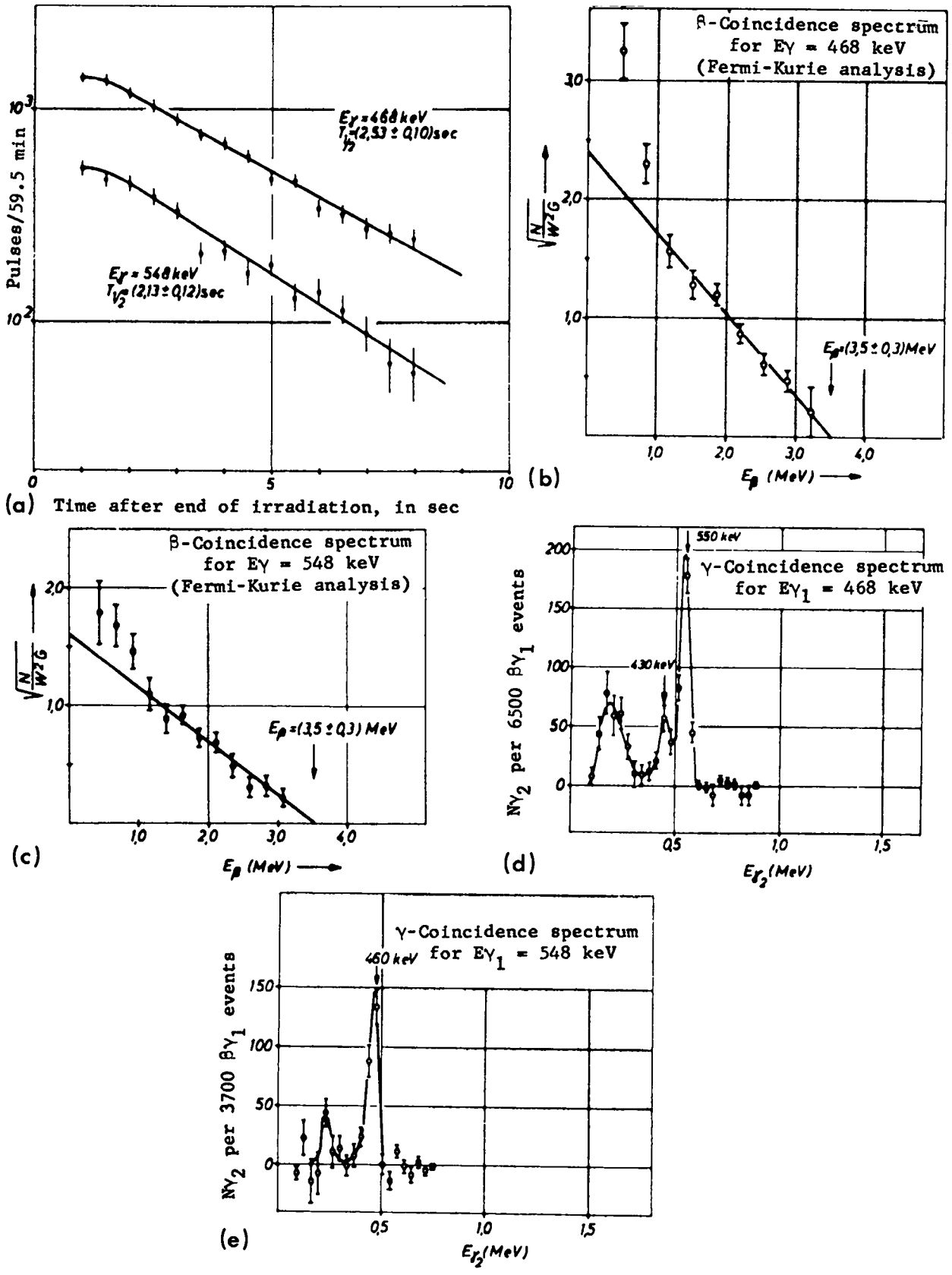

Fig. 24. Decay curves, β-coincidence spectra, and γ-coincidence spectra for the 468- and 548-keV lines of ^{99}Zr.

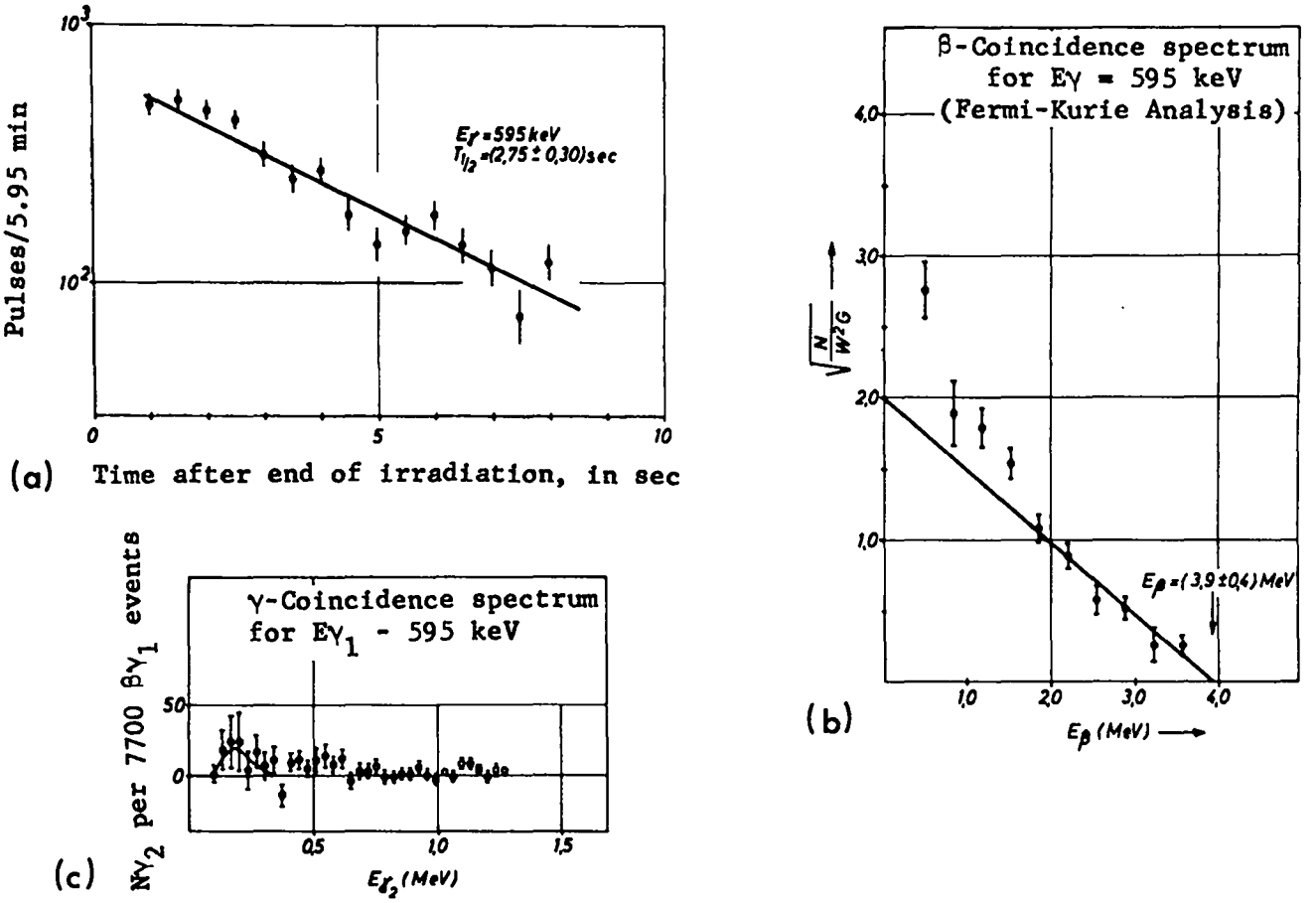

Fig. 25. Decay curve, β-coincidence spectrum, and γ-coincidence spectrum for the 595-keV line of ^{99}Zr.

follows: 3.5 ± 0.3 MeV for the 468-keV line, Fig. 24(b); 3.5 ± 0.3 MeV also for the 548-keV line, Fig. 24(c); and 3.9 ± 0.4 MeV for the 595-keV line, Fig. 25(b). The 548-keV line is clearly visible in the 468-keV γ-coincidence spectrum, Fig. 24(d); conversely, the 468-keV line is clearly visible in the 548-keV γ-coincidence spectrum, Fig. 24(e). In addition to the 548-keV line, another, four times weaker, line at 430 ± 20 keV is observed in Fig. 24(d). In Fig. 24(e) this latter line is either absent or obscured by the 468-keV line. The 595-keV γ-coincidence spectrum in Fig. 25(c) shows no coincident line of significant strength.

According to the assumptions about primary nuclear charge, Z_p, the cumulative yield of ^{99}Zr is about 90% of chain yield. This is in sharp contradiction to the test value of Troutner et al.[43] who report an upper limit of 3%. If this low yield were correct, it would mean a gross deviation of the Z_p curve. However, the existence of the molybdenum isotopes 103 through 107 as fission products was experimentally confirmed by Kienle et al.[55,56] and Feuerstein,[57] which speaks clearly against a break in the Z_p curve. Therefore we adopt the value of 90% for the cumulative yield of ^{99}Zr. The measured line intensities indicate a yield about half that of the chain yield for both the 468- and 548-keV lines, whereas a yield of about 40% of chain yield is obtained for the noncoincident 595-keV line. Accordingly, about half of the ^{99}Zr decay events take place over the γ-γ cascade, and about half through the 595-keV line. From these line yields and from the half-life, the 3.5- and 3.9-MeV β transitions are found to have log ft's of about 4.1 and about 4.4, respectively. Therefore both are allowable trans-

itions.

The fact that the coincident 468- and 548-keV lines have the same yield and that their coincident β energies are identical, leads to the conclusion that only the upper level, not the middle level also, is filled by β decay in the γ-γ cascade. From the energy sum of the 1016-keV cascade and the average 3.5 ± 0.2-MeV β energy, we compute Q as 4.5 ± 0.2 MeV. With the 3.9 ± 0.4-MeV β energy, we obtain a 4.5 ± 0.2-MeV Q for the 595-keV line. We conclude from the exact agreement of the two Q values, that both the cascade and the single line end in the same level of ^{99}Nb. According to the results of Sec. 7.4, decay in the fission-product mass chain takes place almost exclusively through the 14-sec ^{99}Nb ground state. Accordingly, the almost equal yield of cascade and single line speaks against one of the two transitions leading to the 2.4-min ^{99}Nb isomer. Half-life analysis of the 137-keV line of 14-sec ^{99}Nb in Sec. 7.4 gave a rough estimate of 5 ± 2 sec for the ^{99}Zr lifetime, which is compatible with the measured 2.4 ± 0.1-sec half-life. The Q for ^{99}Zr decay to 14-sec ^{99}Nb is obtained by averaging the above test values as 4.5 ± 0.2 MeV. This fits well into the Q-value system for even-odd nuclei (Fig. 13).

The sequence of the two lines in the γ-γ cascade is open at first. We have confirmed that above the 595-keV level, which is being emptied by the single line, there is a 1016-keV level corresponding to the cascade sum. The 421-keV energy difference is identified with the weak γ line observed at about 430 keV. But if the 430-keV line were to originate at the 1016-keV level, then the 468-keV line could not also start at this level because the 430-keV line is coincident with the 468-keV line. According to this reasoning, the 468-keV line must be the lower line in the cascade. With this solution, it remains unclear why the 430-keV line does not appear lightly in the 595-keV γ-coincidence spectrum as the decay mode demands in this case. Possibly, the statistical data are inadequate. Furthermore, between the 595- and 468-keV levels there must be another 127-keV transition also coincident with the 468-keV line. It cannot be observed, because in the γ-γ coincidence spectrum, Fig. 24(d), it falls below the electronic threshold of the two-dimensional equipment.

Figure 26 shows a proposal for the ^{99}Zr decay mode resulting from these considerations. The 2.4-min ^{99}Nb isomer which should be located several hundred keV above the ^{99}Nb ground state is not significantly populated by decay, and, for simplicity, is therefore not shown in Fig. 26. In Sec. 7.4, the ^{99}Nb ground state was assigned $9/2^+$ spin and parity. It is difficult to extimate spin for ^{99}Zr. Even for ^{97}Zr (see Sec. 7.3), Cohen's test value[42] does not agree with that obtained from simple application of shell-model systematics.

7.6. Niobium-100

The 159 ± 3-keV line from Table III (Sec. 4.4) was attributed to ^{100}Nb. Orth and Smith[47] identified ^{100}Nb from among fission products, and measured its half-life as 3.0 ± 0.3 min. They attributed to this nuclide a strong 530-keV γ line that appears in coincidence with lines at 140, 360, 450, 530, and 650 keV. Their attempt to observe this 3-min niobium activity by ^{100}Mo(n,p) reaction was unsuccessful. After bombarding natural molybdenum with fast neutrons, Takahashi et al.[58] separated a 12-min niobium activity which they attributed to ^{100}Nb. They observed γ lines of 530, 620, 1040, 1150, and 1470 keV. In Ref. 18 it is

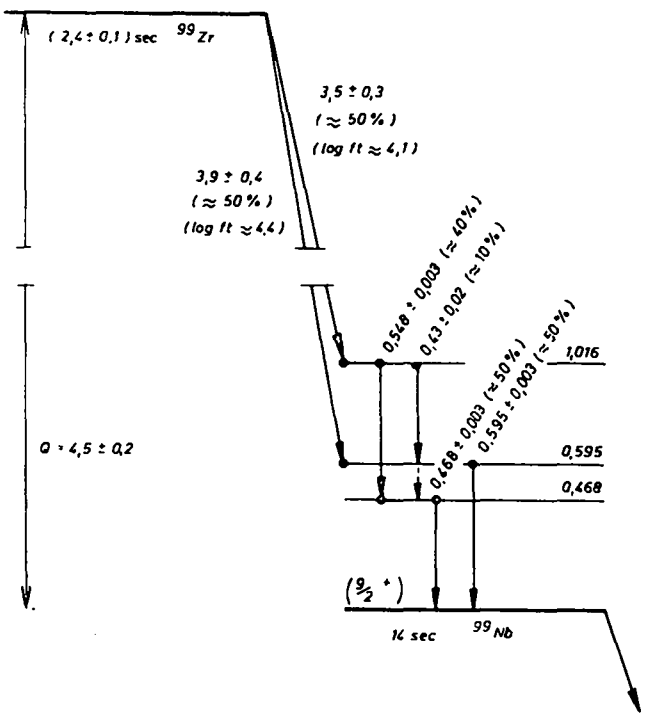

Fig. 26. Proposed ^{99}Zr decay mode.

presumed that Orth and Smith, on the one hand, and Takahashi et al.[58] on the other, measured the same state of ^{100}Nb, and that the large differences in half-life are due to contamination. Huebenthal[49,50] determined a half-life of 2.5 ± 0.3 sec for ^{100}Nb by ^{100}Mo(n,p) reaction. He found strong γ lines at 157, 533, and 598 keV and weak γ lines at 360 and 400 keV. Like Orth and Smith, he could not detect a long-lived ^{100}Nb isomer with a half-life of several minutes after the (n,p) reaction. Kaffrell et al.[51] used the same reaction and found, like Huebenthal, a half-life of 2.2 sec. The corresponding γ spectrum shows strong lines at 162.3, 536.2, and 601.0 keV. Gujrathi and Mukherjee,[59] however, attributed a 2.8 ± 0.2-min activity, which they found on irradiating ^{100}Mo with fast neutrons, to ^{100}Nb. Guzzocrea et al.,[60] who performed an analogous investigation, described the situation as very complicated and did not make any assignments even though they had performed γ spectroscopy and β-γ coincidence measurements. They pointed out that in irradiating ^{100}Mo specimens they found a 3-min activity due to contamination by silver.

In the β-γ-γ coincidence measurements (see Sec. 5.3) for the 159-keV line, a strong coincident line was found at 540 ± 20 keV (see Fig. 27(c)). This line was identified with a 533 ± 3-keV line already known from systematic search for strong γ lines. It was not included in Table III because its Bρ distribution seemed to show indications of admixture of a second line of equal energy with adjacent mass. The γ- and β-coincidence spectra for 533 keV were not measured. Fermi-Kurie analysis of the 159-keV β-coincidence spectrum, Fig. 27(b), yields a β energy of 5.3 ± 0.3 MeV.

The Bρ value of the 159-keV line corresponds to a mass of 100.9 ± 0.7. The Bρ distribution of the 533-keV line yields a mass of 100.2 ± 1.1. Since only a small portion of ^{100}Nb is of primary origin, this nuclide should theoretically appear at mass 100.0.

Figure 27(a) shows the half-life analysis of the 159-keV line. The value found is 6.5 ± 0.3 sec. The curve for the coincident 533-keV line plotted in the same figure yields a value of 6.7 ± 0.3 sec. The average for both measurements is 6.6 ± 0.2 sec. Agreement with the results of Huebenthal[49,50] and Kaffrell et al.[51] is poor. However, both authors' values were obtained by recording the 530-keV line decay curve by means of a single-channel discriminator. This curve was then resolved into two components: because of oxygen contamination at the targets, a 7.4-sec activity originating from ^{16}N produced in the ^{16}O(n,p) reaction was subtracted. Development of 7.4- and 6.6-sec activities could easily have produced errors in these authors' studies.

On the other hand, we should discuss the possibility that Huebenthal's 2.5-sec value for ^{100}Nb is correct and that the 6.6-sec half-life is simulated by decay of the parent nuclide, ^{100}Zr. For this purpose we must examine the ratio of the yield rates and the irradiation time selected. If we assume a Z_p curve according to Sec. 2.4, ^{100}Nb would have a primary yield of about 35%, and ^{100}Zr a cumulative yield of about 65%, of chain yield. Then the ^{100}Zr would have to have a half-life of 6.0 ± 0.5 sec to simulate an average 6.6-sec half-life for a 2.5-sec daughter in the test interval. However, in semilogarithmic scale this decay curve would have slight but noticeable curvature which would show in the statistical data for the two test curves in Fig. 27(a). For this reason, we maintain the 6.6-sec test value as representing the correct ^{100}Nb half-life. Because of the absence of curvature and with the given production rates, the half-life of ^{100}Zr can be only 1.0 ± 0.9 sec.

Further, we consider the available data on excited levels in the daughter nucleus, ^{100}Mo, in preparing a decay mode as proposed in Fig. 28. By Coulomb excitation with α particles, Stelson and McGowan[61] confirmed for this even-even nucleus the presence of a second 2^+ vibrational level at 1050 keV in addition to a first 2^+ level at 530 keV. The former decays through a γ-γ cascade of 520 ± 5 and 530 ± 5 keV. In a later study Robinson, Stelson, McGowan, et al.,[62] observed γ radiation of 535.5 ± 0.3 keV during precision measurement. By use of the (d,d') reaction, Kim and Cohen[63] found excited levels for ^{100}Mo at 540 and 1960 keV and above.

Stelson and McGowan's coincidence experiments[61] and those of Orth and Smith[47] lead to the

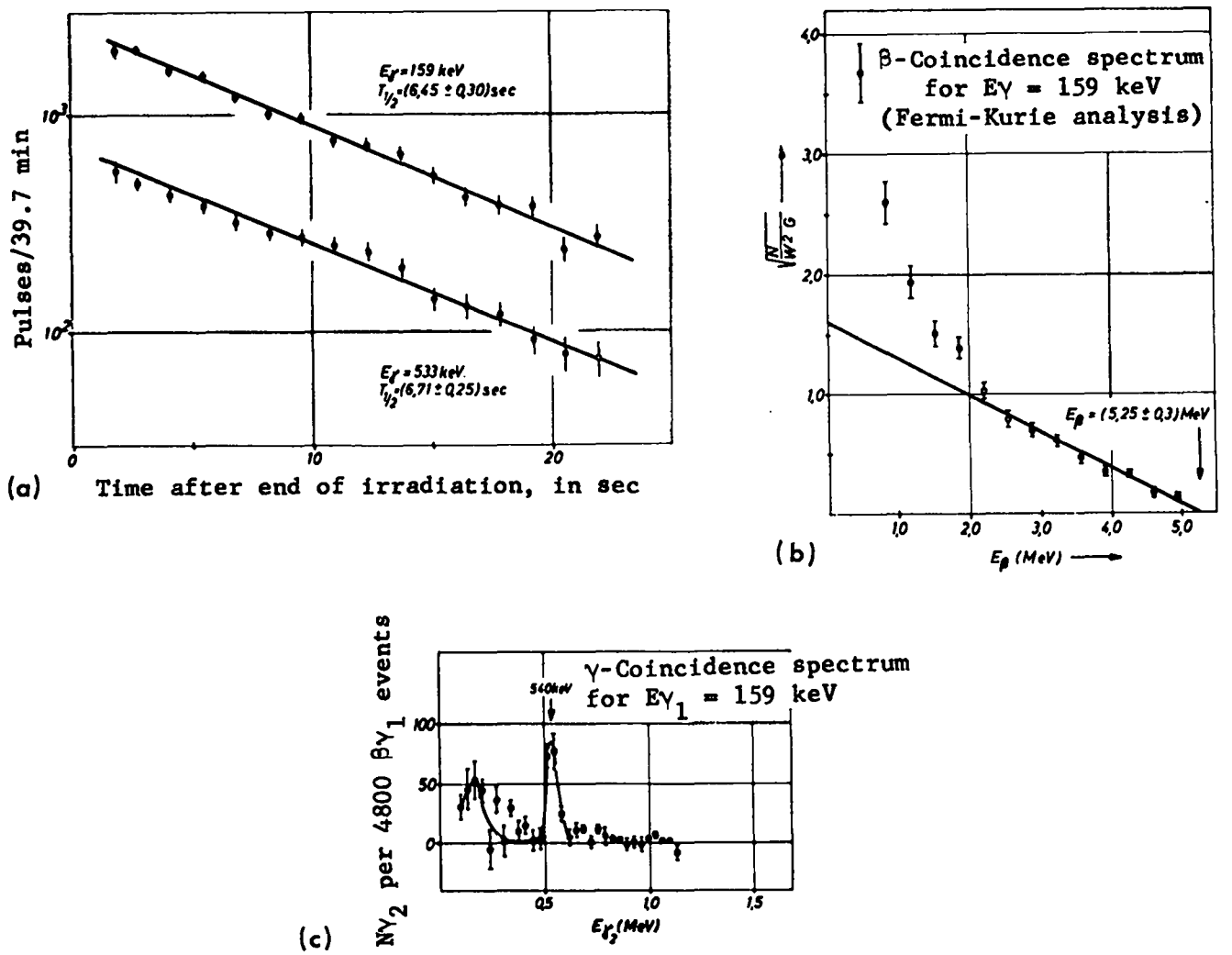

Fig. 27. Decay curves for the 159- and 533-keV lines, and β- and γ-coincidence spectra for the 159-keV line of ^{100}Nb.

conclusion that the 533-keV line observed occurs twice in the decay mode as a member of a cascade. However, for lack of the 533-keV γ-coincidence spectrum, we cannot confirm this by experiment. No line with adjacent energy, e.g., 520 keV, appears in the β-γ spectra during systematic search (Sec. 4.4). The measured intensity of the 533-keV line, which is of the magnitude of the chain yield, is therefore distributed among the two lines of the cascade, giving a yield of 50% of chain yield. Computation from the intensity of the 159-keV line also gives a yield of 50% of chain yield. The cumulative yield of ^{100}Nb is about 100% of chain yield. From the 50% yield and the half-life measured, log ft for the 5.3-MeV β transition is found to be 5.2. Therefore the transition is allowable.

The 159-keV line, for which coincidence with 533 keV is confirmed, Fig. 27(c), might be identical with Orth and Smith's 140-keV coincidence line, Huebenthal's 157-keV line, and the 162-keV line of Kaffrell et al. From the line yields, we assume that this line fills the level Stelson and McGowan found at about 1050 keV. For the energy of this level, we will adopt the sum of the 535.5-keV test value of Robinson et al. and of our 533-keV test value.

Based on these considerations, the decay Q value is composed of the triple γ cascade (535.5 + 533 + 159 keV) and of the β energy coincident to 159 keV (5.3 MeV). This leads to a value of 6.5 ± 0.3 MeV which fits well into the Way-Wood diagram for odd-odd nuclei (Fig. 12).

Although the ground state of the ^{100}Mo even-even nuclei has 0^+ spin and parity and the first

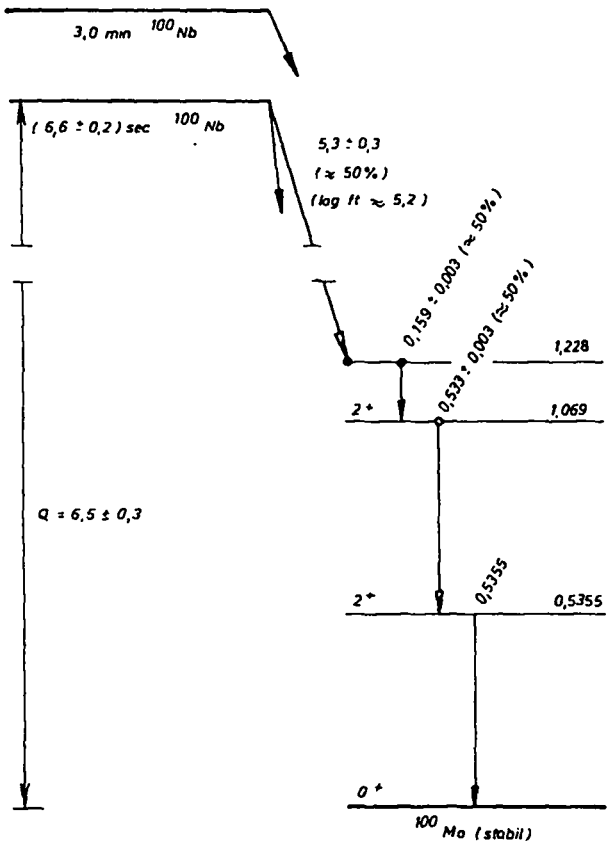

Fig. 28. Proposed ^{100}Nb decay mode.

two excited levels are known as 2^+, it is difficult to make any prediction for the third level, which is filled by β decay, because spin and parity for the 6.6-sec state of the ^{100}Nb odd-odd nucleus are unclear.

We cannot clarify whether the 3.0-min state of ^{100}Nb, which Orth and Smith also observed in fission, represents the ground state or an isomeric excitation level. It is equally uncertain whether this 3.0-min state is located above or below the 6.6-sec state. It is without any clue, that it is drawn in the proposals for the decay mode, Fig. 29(a). Finally, the question remains as to how the remaining 50% of the yield is distributed over a possible ground state transition which empties the 6.6-sec state, or over the decay originating from the 3.0-min state.

7.7. Niobium-101

The lines listed in Table III (Sec. 4.4) at 273 ± 3 and 399 ± 3 keV both had to be attributed to ^{101}Nb although they do not coincide. Orth and Smith[47] reported a half-life of 1.0 ± 0.2 min for this nuclide. They separated niobium from a fission product mix and determined half-life by "milking."

Mass values obtained from the Bρ positions are 101.7 ± 0.7 for the 273-keV line and 100.4 ± 0.6 for the 399-keV line. The theoretical ^{101}Nb value derived from apparent mass shift (Sec. 2.4) is 101.4 ± 0.3.

Figure 29(a) shows the half-life analysis of the 273-keV line, and Fig. 30(a) shows that of the 399-keV line. The results are 7.2 ± 0.3 and 6.7 ± 9.3 sec which gives an average of 7.0 ± 0.2 sec. Accordingly, this cannot be the same state of ^{101}Nb that Orth and Smith observed. From the different initial curvatures of the two decay curves, Figs. 29(a) and 30(a), the half-life of the parent nuclide, ^{101}Zr, may be roughly estimated at about 1.5 or 3 sec.

Figures 29(b) and 30(b) show the Fermi-Kurie diagrams of the respective coincident β spectra. The β energy of the 273-keV line is found to be 4.3 ± 0.25 MeV and that of the 399-keV line, 4.1 ± 0.7 MeV. The γ-γ coincidence spectra, Figs. 29(c) and 30(c), show that neither of the two lines coincides with a strong line.

From the assumptions about primary charge distribution in Sec. 2.4, it follows that ^{101}Nb has a cumulative yield of about 95% of chain yield. From the line intensities, we compute the 273-keV line yield as about 60% of chain yield, and that of the 399-keV line as about 30%. Accordingly, at least about 90% of the decay events in the 101 mass chain take place over the 7.0-sec state of ^{101}Nb investigated. Using the estimated line yields and the measured half-life, we give log ft for the two β transitions as about 4.9 or 5.0. Accordingly, allowable β decay events are involved.

In the decay-mode proposal advanced in Fig. 31, Hjorth and Cohen's[53] data on excitation levels in the daughter nucleus, ^{101}Mo, determined by the ^{100}Mo(d,p) reaction will be considered further. In contrast to the ^{99}Mo data in Sec. 7.4 for the ^{99}Nb decay mode, the reaction data for this nuclide are rather inaccurate because the energies of the lower six levels were obtained by generation of double peaks. Hjorth and Cohen list the following excitation states: ~60, ~260, ~310, and ~470 keV and additional higher levels. Considering the rela-

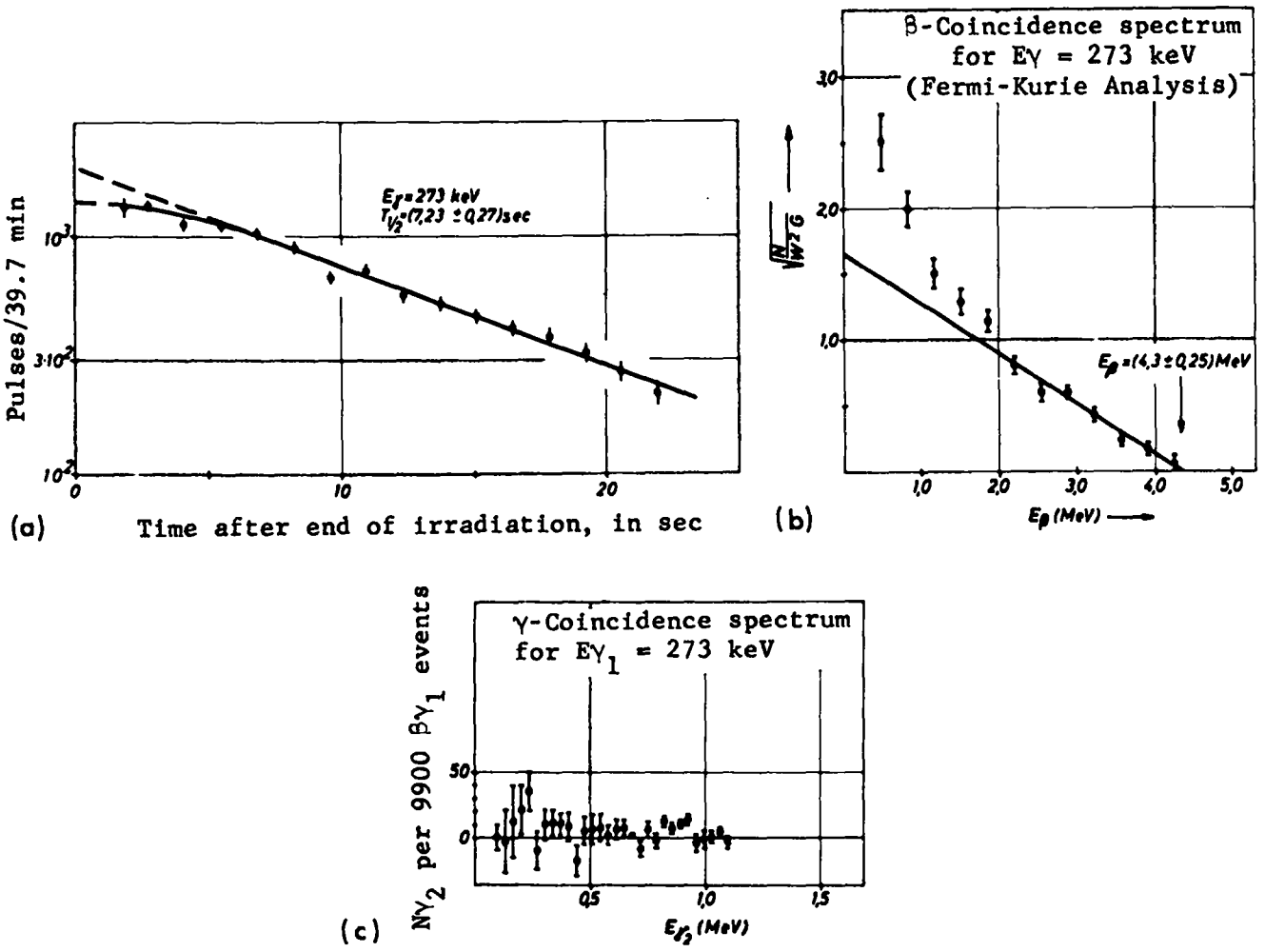

Fig. 29. Decay curve, β-coincidence spectrum, and γ-coincidence spectrum for the 273-keV line of ^{101}Nb.

tively large inaccuracy in these energy data, the 273-keV line fits fairly well into the 310- to 60-keV energy difference, and the 399-keV line into the 470- to 60-keV difference. With this assignment, both γ lines fill the level at about 60 keV. But a γ line of about 60 keV was not observed. In the γ-γ coincidence spectra, it would certainly fall below the electronic threshold, but it should have been observed in the systematic recording of the β-coincident γ spectra. Either the line is strongly converted, or the 60-keV level has a lifetime longer than the 0.2-sec coincidence resolution time. The second solution is preferred because of analogy to ^{99}Mo for which a 13-μsec isomer is known at 98 keV. We assume that this involves the 13-μsec isomer with 44 keV, which McCarthy et al.[54] observed during deuteron irradiation of natural molybdenum, as well as the 98-keV isomer of ^{99}Mo. This assignment of the 44-keV isomer to ^{101}Mo is at least as probable as its assignment to ^{99}Mo by Huebenthal[49,50] (see Sec. 7.4).

The decay Q value would then be as follows: the 4.3 ± 0.25-MeV coincident β energy is to be added to the sum of 44 and 273 keV, giving a Q of 4.6 ± 0.25 MeV. On the other hand, the 4.1 ± 0.7-MeV β energy is to be added to 44 and 399 keV, giving a Q of 4.5 ± 0.7 MeV. The average Q is 4.6 ± 0.2 MeV which fits well into the Way-Wood diagram for odd-even nuclei (Fig. 14).

Hjorth and Cohen's spin assignments[53] for the ^{101}Mo excitation levels are uncertain, as are the energy values. However, they stress that the value of $1/2^+$ for the ^{101}Mo ground state is sub-

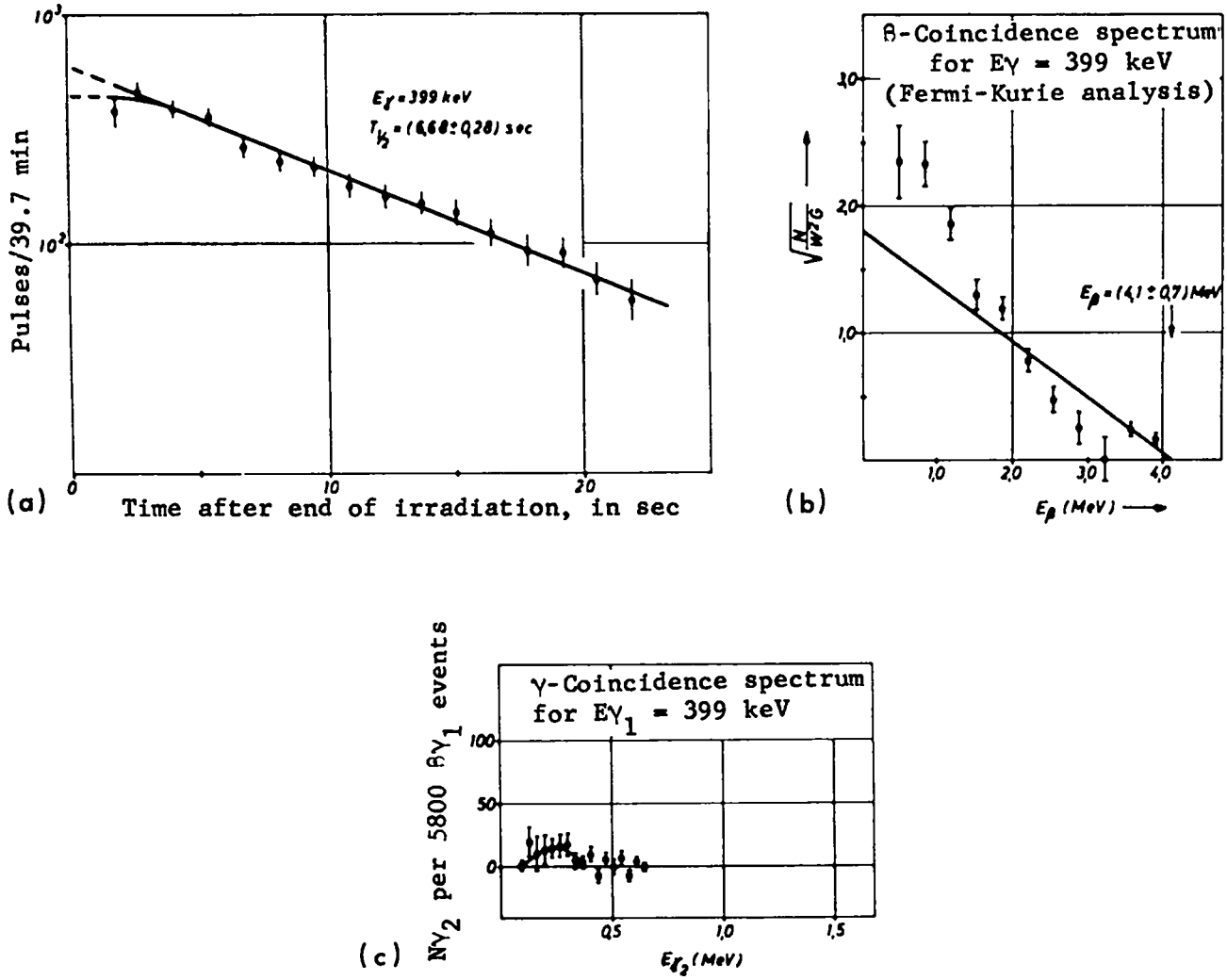

Fig. 30. Decay curve, β-coincidence spectrum, and γ-coincidence spectrum for the 399-keV line of ^{101}Nb.

stantiated. The spin assignments obtained from rough estimates of the peak heights and angle distributions contradict the conclusions to be drawn from the allowable β decay. Considering the shell model (see also Sec. 7.4), only $9/2^+$ and $1/2^-$ are possible for spin and parity in ^{101}Nb. As in the case of all odd niobium isotopes, the $1/2^-$ configuration is attributed to an isomeric level several hundred keV above the ground state. Analogous to ^{99}Nb, it would here be the longer-lived state, i.e., the 1.0-min state found by Orth and Smith.[47] Therefore the 7.0-sec ^{101}Nb ground state is of $9/2^+$ configuration. Allowed β transitions can then lead only to levels with $7/2^+$, $9/2^+$, or $11/2^+$. However, Hjorth and Cohen assigned different spin values to their levels at ~310 and ~470 keV. From comparison with the ^{99}Mo isomeric level and the ^{105}Pd ground state, a $5/2^+$ configuration is probable for the isomeric level at 44 keV, which again contradicts the spin reported by Hjorth and Cohen at about 60 keV. As for ^{99}Mo, the isomeric level would then emit E2 radiation. For the 273- and 399-keV lines, the $11/2^+$ to $5/2^+$ transition would have to have at least the multipole order M 3. But the corresponding lifetime is large compared to the 0.2-μsec coincidence resolution time, so the lines would not have been found. Accordingly, the $11/2^+$ configuration for the two levels filled by β decay is not possible. By comparison, the $9/2^+$ to $5/2^+$ transition in the

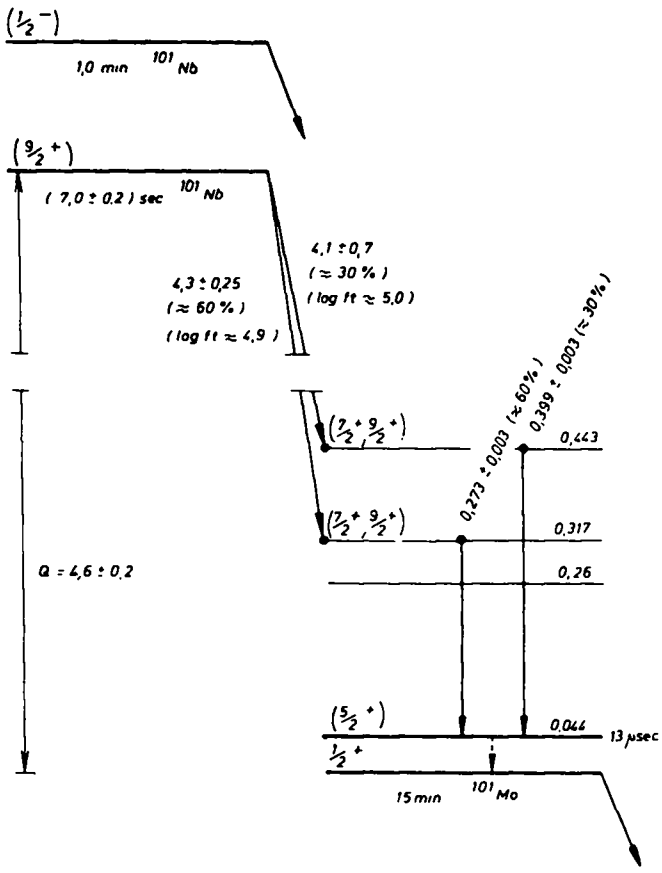

Fig. 31. Proposed ^{101}Nb decay mode.

form of E2 radiation corresponds to a lifetime of 10^{-8} to 10^{-7} sec for these levels, so that the assignment of $9/2^+$ cannot be excluded.

7.8. Zirconium-101

The 293 ± 3-keV line was attributed to ^{101}Zr. The literature does not furnish any data on this nuclide.

The Bρ value of the line corresponds to a mass of 102.0 ± 0.6. Theoretically, the value of 102.5 ± 0.6 would be expected for ^{101}Zr which, as a nuclide of primary origin, is subject to apparent mass shift.

Figure 32(a) shows the decay curve for the 293-keV line as given by half-life analysis. The result is 3.3 ± 0.6 sec. The statistical accuracy of the decay curve is only moderate; therefore the error is relatively large compared to other half-life analyses. The curve shows no initial curvature. However, the yield of the parent nuclide, ^{101}Y, is so small that its half-life cannot be estimated on the basis of this behavior. The 3.3-sec half-life measured for ^{101}Zr agrees with the estimated 1.5 to 3.0 sec obtained from the initial curvature of the ^{101}Nb decay curves (Sec. 7.7).

Figure 32(b) shows the β spectrum coincident to 293 keV in the form of a Fermi-Kurie diagram. Analysis gives a β energy of 6.1 ± 0.7 MeV. The γ-γ coincidence spectrum, Fig. 32(c), contains a 400 ± 20-keV line coincident to 293 keV. Its yield is about 7 times less than that of the 293-keV line. The stronger line must be the lower line in the γ-γ cascade.

It follows from the assumptions regarding primary nuclear charge distribution (see Sec. 2.4) that the cumulative yield for ^{101}Zr is about 50% of chain yield. The 293-keV line intensity corresponds to a yield of about 50% of chain yield. Accordingly, practically all ^{101}Zr decay events take place above the 293-keV level. A yield of about 15% of the nuclide decay events for the 400-keV line follows. A yield of 85% remains for the β transition that fills the 293-keV level. Its energy spectrum is overlapped by lower energy β transitions which lead through the 690-keV level (293 keV + 400 keV). This effect is estimated as about 0.1 MeV. Thus, 6.2 ± 0.7 MeV is considered the β energy coincident to 293 keV. The corresponding value of log ft is about 5.0. Accordingly, the β decay is allowable.

The decay Q value is given by the sum of 293 keV and 6.2 MeV as 6.5 ± 0.7 MeV, which agrees with extrapolations of the Way-Wood lines which may be performed for the even-odd nuclei in Fig. 13.

Figure 33 presents the proposed ^{101}Zr decay mode. The 7.0-sec ^{101}Nb ground state is considered to be the daughter nucleus from this decay. The results of Sec. 7.7 indicate that no significant part of the decay can occur over the 1.0-min isomer. Since we do not know how far this isomer is above the ground state, we do not show it in the decay mode for reasons of simplicity. In Sec. 7.7, spin and parity of the 7.0-sec ^{101}Nb were assumed to be $9/2^+$. We cannot discuss ^{101}Zr spin and parity for the reasons given in the case of ^{99}Zr (see Sec. 7.5).

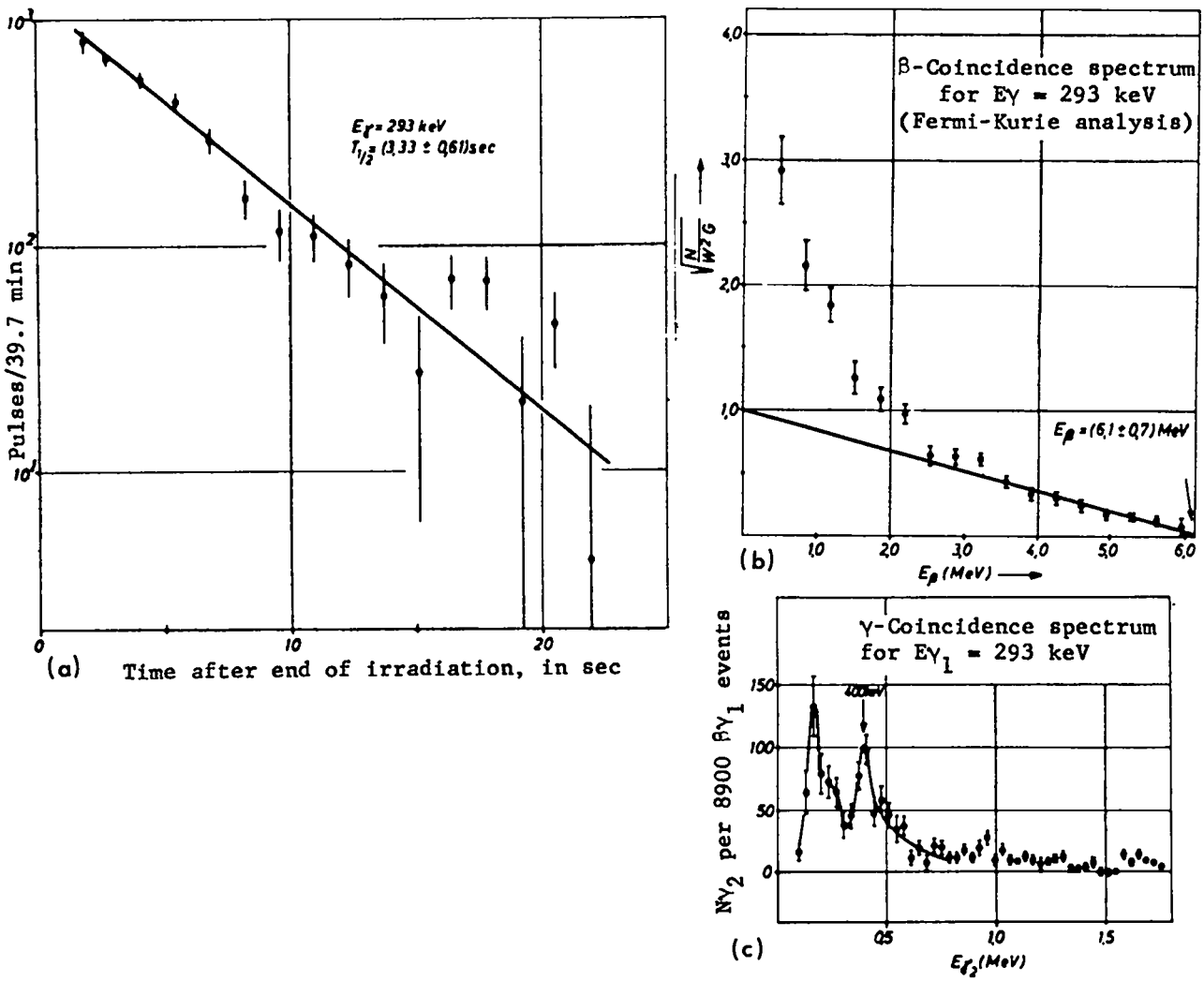

Fig. 32. Decay curve, β-coincidence spectrum, and γ-coincidence spectrum for the 293-keV line of ^{101}Zr.

ACKNOWLEDGMENTS

I am indebted to Dr. P. Armbruster, Director of the Department of Solid State Physics and Nuclear Physics of the Jülich Nuclear Research Center, who suggested and guided this study, for his constant supporting interest and numerous valuable discussions.

I am especially indebted to E. Roeckl, graduate physicist, for his cooperation in the construction of the mass separator and for his assistance in performing the tests.

For several tedious test series, I enjoyed the assistance of J. W. Grueter, graduate physicist, and Messrs. H. Lawin and K. Sistemich.

Messrs. H. Labus and H. J. Stein assisted in construction and maintenance of electronic equipment. Dr. F. Hossfeld assisted in computer analysis of test data. I am indebted to all.

I am indebted to Mr. T. Kuenster, who was assigned to the mass separator as operator, for his conscientious work in construction and maintenance of test equipment. The prerequisite for all measurements was reliable operation of the Jülich FRJ-2 research reactor, for which I am indebted to the staff of the Central Division for Research Reactors of the Nuclear Research Center.

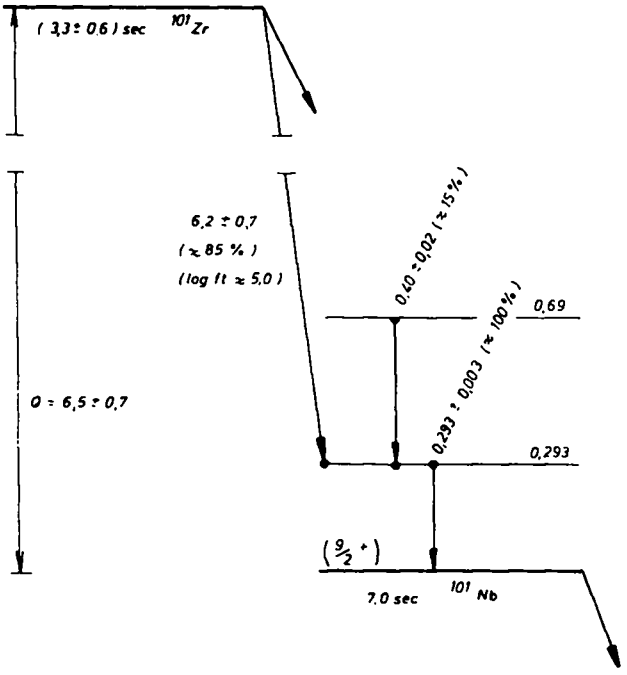

Fig. 33. Proposed ^{101}Zr decay mode.

REFERENCES

1. I. Bergstroem, Nucl. Instr. Meth., 43, 116 (1966).
2. "Why and How Should We Investigate Nuclides Far Off the Stability Line," Proc. Lysekil Symp. (1966), Arkiv Fysik, 36 (1967).
3. H. Seyfarth, Nukleonik, 10, 193 (1967).
4. B. L. Cohen and C. B. Fulmer, Nucl. Phys., 6, 547 (1958).
5. P. Armbruster, Nukleonik, 3, 188 (1961).
6. P. Armbruster, J. Eidens, and E. Roeckl, Proc. Lysekil Symp., Arkiv Fysik, 36, 293 (1967).
7. H. H. Heckman, E. L. Hubbard, and W. G. Simon, Phys. Rev., 129, 1240 (1963).
8. H. D. Betz, G. Hortig, E. Leischner, Ch. Schmelzer, B. Stadler, and J. Weihrauch, Phys. Lett., 22, 643 (1966).
9. D. Hovestadt, Ph.D. Thesis, College of Technology, Munich (1964).
10. D. Hovestadt and P. Armbruster, Nukleonik, 9, 338 (1967).
11. D. Hovestadt, P. Armbruster, and J. Eidens, Z. Phys., 178, 226 (1964).
12. J. W. Grueter, Master's Thesis, College of Technology, Aachen (1968).
13. A. C. Wahl, "Physics and Chemistry of Fission," Proc. Salzburg Symp. on Physics and Chemistry of Fission, Salzburg, 1965, IAEA, Vienna, 1, 317 (1965).
14. J. C. D. Milton and J. S. Fraser, Proc. Salzburg Symp. on Physics and Chemistry of Fission, Salzburg, 1965, IAEA, Vienna, 2, 39 (1965).
15. W. Reisdorf, Z. Physik, 209, 77 (1968).
16. W. Reisdorf and P. Armbruster, Phys. Lett., 24B, 501 (1967).
17. P. Armbruster and H. J. Specht, Nukleonik, 4, 283 (1962).
18. Nuclear Data Sheets (1959-1965), or Nuclear Data Section B (1966-1967), Academic Press, New York and London.
19. V. Cojocaru and M. Nachman, IFA-NR-24 (1966).
20. J. E. Kitching and M. W. Johns, Can. J. Phys., 44, 2661 (1966).
21. J. E. Kitching and M. W. Johns, Nucl. Phys., A98, 337 (1967).
22. R. H. Goodman, J. E. Kitching, and M. W. Johns, Nucl. Phys., 54, 1 (1964).
23. M. A. Wahlgren and W. W. Meinke, J. Inorg. Nucl. Chem, 24, 1527 (1962).
24. V. Akamian, USNRDL-TR-733 (1964).
25. P. Kienle, K. Wien, U. Zahn, and B. Weckermann, Z. Physik, 176, 226 (1963).
26. C. E. Bemis, V. Berg, K. Fransson, and T. Alvaeger, Arkiv Fysik, 30, 486 (1965).
27. K. Fritze and T. J. Kennett, Phys. Rev., 127, 1262 (1962).
28. (Nuclide Chart), Second Edition (Second Reprint 1965), Department of Radiochemistry, Nuclear Research Center, Karlsruhe.
29. Preprint to be published in J. Inorg. Nucl. Chem.
30. P. del Marmol and M. Neve de Mevergnies, J. Inorg. Nucl. Chem., 29, 273 (1967).
31. L. Tomlinson, in "Delayed Fission Neutrons," Proceedings of a Panel, IAEA, Vienna (1967), p. 61.
32. I. Amarel, R. Bernas, R. Foucher, J. Jastrzebski, A. Johnson, J. Teillac, and H. Gauvin, Phys. Lett., 24B, 402 (1967).

32a. H. Gauvin, Private communication to P. del Marmol.

33. P. Patzelt and G. Herrmann, Proc. Salzburg Symp. on Physics and Chemistry of Fission, Salzburg, 1965, IAEA, Vienna, 2, 243 (1965).
34. K. Huebenthal, J. Berthier, J. Hocquenghem, and A. Moussa, Compt. Rend. Acad. Sci., Paris, 265B, 162 (1967).
35. J. E. Sattizahn, J. D. Knight, and M. Kahn, J. Inorg. Nucl. Chem., 12, 206 (1960).
36. S. Amiel, J. Gilat, A. Notea, and E. Yellin, Proc. Lysekil Symp. on Nuclides Far Off Stability Line, Lysekil, Sweden, 1966, Arkiv Fysik, 36, 169 (1967).
37. S. Borg, U. Faegerquist, G. Holm, and F. Kropff, Nucl. Instr. Meth., 38, 296 (1965).
38. O. Kofoed-Hansen and K. O. Nielsen, Kgl. Danske Videnskab. Selskab, Mat. Fys. Medd., 26, 7 (1951).
39. A. C. Wahl, R. L. Ferguson, D. R. Nethaway, D. E. Troutner, and K. Wolfsberg, Phys. Rev., 126, 1112 (1962).

40. L. H. Niece, D. E. Troutner, and R. L. Ferguson, in ORNL 3832, 26 (1965).

41. L. H. Niece, ORNL-Tm-1333 (1965).

42. B. L. Cohen, Phys. Rev., 125, 1358 (1962).

43. B. L. Cohen and O. V. Chubinsky, Phys. Rev., 131, 2184 (1963).

44. R. E. Larson and C. M. Gordon, Nucl. Phys., 88, 481 (1966).

45. J. van Klinken, L. M. Taff, G. W. Eakins, A. J. Bureau, and E. N. Hatch, Phys. Rev., 154, 1116 (1967).

46. R. B. Duffield, L. Hsiac, and E. N. Sloth, Phys. Rev., 79, 1011 (1950).

47. C. J. Orth and R. K. Smith, J. Inorg. Nucl. Chem, 15, 4 (1960).

48. D. E. Troutner, R. L. Ferguson, and G. D. O'Kelley, Phys. Rev., 130, 1466 (1963).

49. K. Huebenthal, Thesis, University of Grenoble (1968).

50. K. Huebenthal, E. Monnand, and A. Moussa, Compt. Rend. Acad. Sci., Paris, 265B, 579 (1967).

51. N. Kaffrell, R. Denig, G. Herrmann, W. Herzog, G. Rosner, and N. Trautmann, Verhandl. DPG (VI) 3, 358 (1968), and private communication.

52. R. B. Duffield and S. H. Vegors, Phys. Rev., 112, 1958 (1958).

53. S. A. Hjorth and B. L. Cohen, Phys. Rev., 135B, 920 (1964).

54. A. L. McCarthy, B. L. Cohen, and L. H. Goldman, Phys. Rev., 137B, 250 (1965).

55. P. Kienle, F. Baumgaertner, B. Weckermann, and U. Zahn, Radiochimica Acta, 1, 84 (1963).

56. P. Kienle, B. Weckermann, F. Baumgaertner, and U. Zahn, Naturwissenschaften (Natural Sciences), 49, 294 and 295 (1962).

57. H. Feuerstein, Kernforschungszentrum, Karlsruhe, report KFK-358 (1965).

58. K. Takahashi, T. Kuroyanagi, H. Yuta, K. Kotajima, K. Nagatani, and H. Morinaga, J. Phys. Soc. Japan, 16, 1664 (1961).

59. S. C. Gujrathi and S. K. Mukherjee, Nucl. Phys., 85, 288 (1966).

60. P. Cuzzocrea, E. Perillo, and S. Notarrigo, Nucl. Phys., A103, 616 (1967).

61. P. H. Stelson and F. K. McGowan, Phys. Rev., 121, 209 (1961).

62. R. L. Robinson, P. H. Stelson, F. K. McGowan, J. L. C. Ford, Jr., and W. T. Milner, Nucl. Phys., 74, 281 (1964).

63. Y. S. Kim and B. L. Cohen, Phys. Rev., 142, 788 (1966).